Report

Cell Reports

A Ubiquitous Platform for Bacterial Nanotube Biogenesis

Graphical Abstract

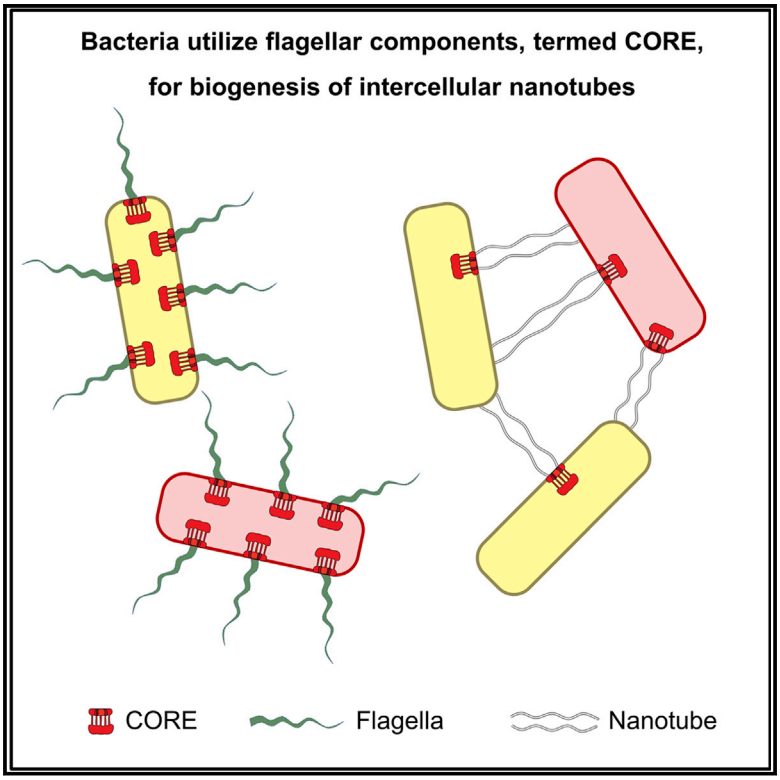

Highlights

- Conserved flagellar CORE components dually serve for flagella and nanotube assembly
- *CORE* mutants are deficient in nanotube formation and intercellular molecular trade
- CORE-dependent nanotube production is conserved among distinct bacterial species
- The CORE-nanotube organelle can provide a common path for bacterial molecular trade

Authors

Saurabh Bhattacharya, Amit K. Baidya, Ritesh Ranjan Pal, ..., Hanah Margalit, Ilan Rosenshine, Sigal Ben-Yehuda

Correspondence

ilanr@ekmd.huji.ac.il (I.R.),
sigalb@ekmd.huji.ac.il (S.B.-Y.)

In Brief

Bhattacharya et al. show that bacterial intercellular nanotubes, facilitating cytoplasmic molecular exchange among cells, emerge from conserved CORE components of the flagellar export apparatus. CORE-mediated nanotube formation is widespread among bacterial species. The results establish the CORE-derived nanotube as a ubiquitous organelle, facilitating intercellular molecular trafficking across the bacterial kingdom.

Bhattacharya et al., 2019, Cell Reports *27*, 334–342
April 9, 2019
https://doi.org/10.1016/j.celrep.2019.02.055

CellPress

OPEN ACCESS
CellPress

Cell Reports
Report

A Ubiquitous Platform for Bacterial Nanotube Biogenesis

Saurabh Bhattacharya,[1,3] Amit K. Baidya,[1,3] Ritesh Ranjan Pal,[1] Gideon Mamou,[1,2] Yair E. Gatt,[1] Hanah Margalit,[1] Ilan Rosenshine,[1,*] and Sigal Ben-Yehuda[1,4,*]

[1]Department of Microbiology and Molecular Genetics, Institute for Medical Research Israel-Canada, The Hebrew University-Hadassah Medical School, POB 12272, The Hebrew University of Jerusalem, 91120 Jerusalem, Israel
[2]Present address: Department of Biochemistry, University of Oxford, South Parks Road, Oxford OX13QU, UK
[3]These authors contributed equally
[4]Lead Contact
*Correspondence: ilanr@ekmd.huji.ac.il (I.R.), sigalb@ekmd.huji.ac.il (S.B.-Y.)
https://doi.org/10.1016/j.celrep.2019.02.055

SUMMARY

We have previously described the existence of membranous nanotubes, bridging adjacent bacteria, facilitating intercellular trafficking of nutrients, cytoplasmic proteins, and even plasmids, yet components enabling their biogenesis remain elusive. Here we reveal the identity of a molecular apparatus providing a platform for nanotube biogenesis. Using *Bacillus subtilis* (*Bs*), we demonstrate that conserved components of the flagellar export apparatus (FliO, FliP, FliQ, FliR, FlhB, and FlhA), designated CORE, dually serve for flagellum and nanotube assembly. Mutants lacking *CORE* genes, but not other flagellar components, are deficient in both nanotube production and the associated intercellular molecular trafficking. In accord, CORE components are located at sites of nanotube emergence. Deleting *CORE*s of distinct species established that CORE-mediated nanotube formation is widespread. Furthermore, exogenous *CORE*s from diverse species could restore nanotube generation and functionality in *Bs* lacking endogenous *CORE*. Our results demonstrate that the CORE-derived nanotube is a ubiquitous organelle that facilitates intercellular molecular trade across the bacterial kingdom.

INTRODUCTION

Bacteria residing in natural communities maintain intricate molecular crosstalk with proximal prokaryotic and eukaryotic cells. Dedicated machineries such as type III, IV, and VI secretion systems are used by bacteria to conduct contact-dependent molecular delivery among species, as well as across kingdoms (Costa et al., 2015; Hayes et al., 2010). We have previously described a type of bacterial contact-dependent interaction mediated by membranous conduits, termed nanotubes, bridging neighboring cells of the bacterium *Bacillus subtilis* (*Bs*) (Dubey and Ben-Yehuda, 2011; Dubey et al., 2016). In fact, nanotube-like structures were shown to be produced by multiple bacterial species, mainly when grown on solid surfaces or in biofilm assemblies (e.g., McCaig et al., 2013; Pande et al., 2015; Wei et al., 2014); however, their function remains mostly elusive. Our previous analysis revealed that nanotubes serve as conduits for an intercellular exchange of cytoplasmic proteins and even plasmids (Baidya et al., 2018; Dubey and Ben-Yehuda, 2011; Dubey et al., 2016; Stempler et al., 2017). Furthermore, we and others reported that nanotubes facilitate interspecies molecular trafficking, including that of nutrients and toxins (Benomar et al., 2015; Pande et al., 2015; Stempler et al., 2017).

Inspired by these results, we recently discovered that enteropathogenic *E. coli* (EPEC) uses nanotubes to interact with infected epithelial cells (Pal et al., 2019). The formation of these nanotubes was dependent on five inner membrane proteins, composing the export apparatus of the type III secretion system (T3SS), embedded within the injectisome, the major virulence machinery of EPEC (Pal et al., 2019). The Gram-positive *Bs* lacks injectisome, which is restricted to Gram-negative pathogens, but its flagellum harbors integral T3SS, including an export apparatus (Abby and Rocha, 2012; Diepold and Armitage, 2015; Diepold and Wagner, 2014). We thus hypothesized that the *Bs* flagellar export apparatus, termed here CORE (CORE-F_{Bs}), is required not only for motility (Hueck, 1998) but also for nanotube generation. The CORE, situated at the basal body of the flagella, is composed of five channel-forming integral membrane proteins, FliP, FliQ, FliR, FlhB, and FlhA, exhibiting a stoichiometry of 5:4:1:1:9, respectively (Dietsche et al., 2016; Fukumura et al., 2017; Kuhlen et al., 2018) (Figure 1A). In addition, FliO, a non-structural component of the CORE, serves as a scaffold for the assembly of FliP multimeric ring, the presumed nucleation step of the CORE complex assembly (Fabiani et al., 2017; Fukumura et al., 2017).

Here we describe that the CORE complex, the central constituent of the bacterial flagellum, has a dual utility, serving as a platform for both flagellum and nanotube biogenesis. We reveal that the CORE is positioned at sites of nanotube emergence, enabling their production along with the associated intercellular molecular exchange. Subsequently, by using bioinformatics and functional analyses, we show that the sequence and utility of CORE components are conserved among distinct bacterial species. Taken together, our results expose the existence of a bacterial organelle related to flagella and injectisome that is likely to

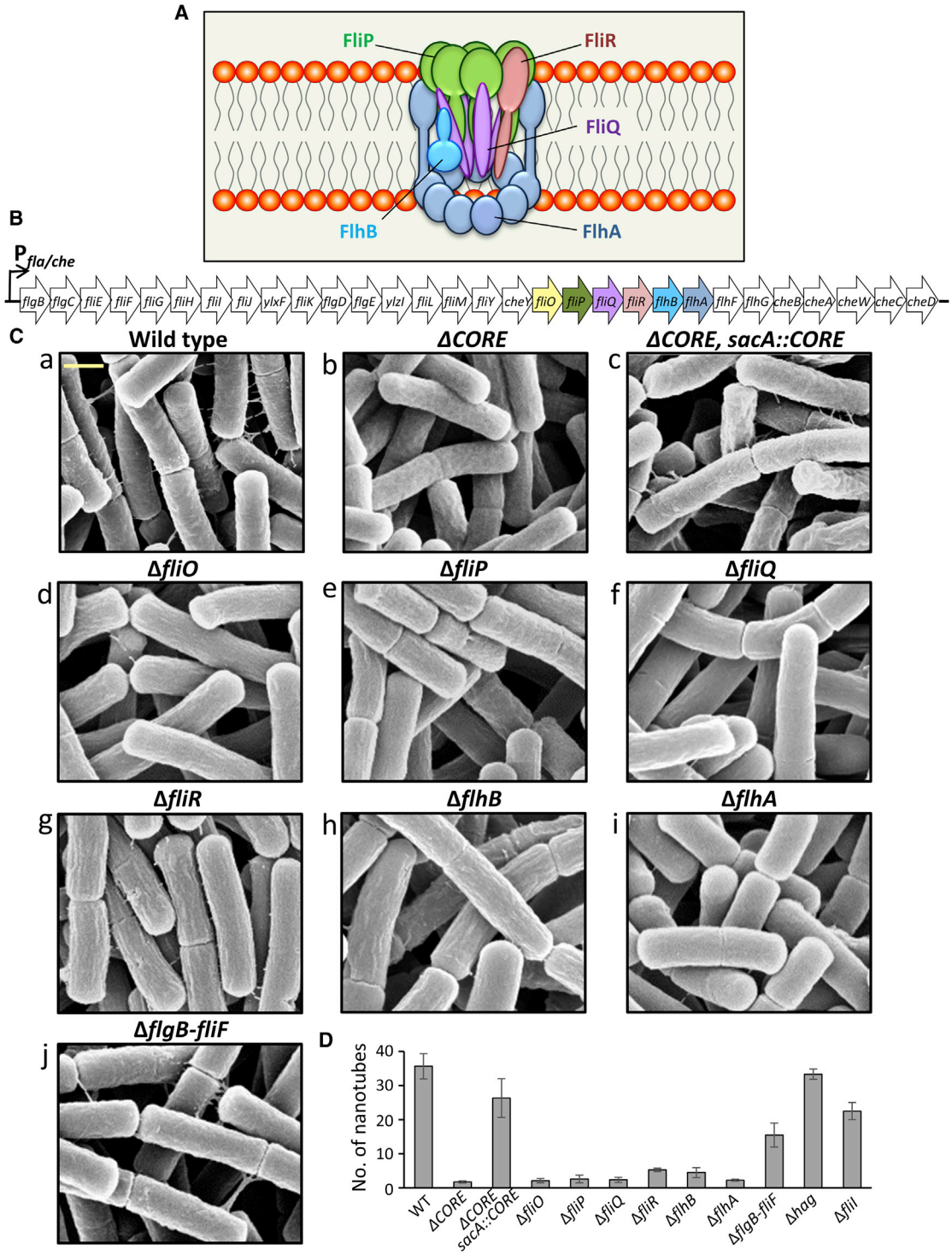

Figure 1. *Bs CORE* Mutants Are Impaired in Nanotube Formation

(A) Schematic illustration of the flagellar CORE apparatus on the basis of Fukumura et al. (2017) and Kuhlen et al. (2018). The CORE consists of FliP, FliQ, FliR, FlhB, and FlhA (5:4:1:1:9) transmembrane proteins and the chaperone FliO (not shown), which only transiently associates with the CORE complex.

(B) A map depicting the *fla/che* operon of *Bs*, encoding the components required for flagellar basal body formation. Genes encoding the CORE proteins are highlighted with the same color code as in (A).

(legend continued on next page)

provide a major and prevalent route for intercellular molecular exchange in bacteria.

RESULTS

Flagellar CORE Proteins Are Required for Nanotube Formation

To investigate whether CORE-F_{Bs} is required for nanotube formation, we generated a non-polar deletion of a chromosomal fragment, containing the five *CORE* genes *fliP*, *fliQ*, *fliR*, *flhB*, and *flhA,* as well as *fliO*, encoding the CORE-associated chaperone (*ΔCORE*) (Figures 1A and 1B) (Fabiani et al., 2017; Fukumura et al., 2017). We then used extreme-high-resolution scanning electron microscopy (XHR-SEM) to examine the capacity of this mutant to form nanotubes on a solid surface, conditions restricting flagella formation and facilitating nanotube biogenesis (Dubey and Ben-Yehuda, 2011). Remarkably, the *ΔCORE* mutant exhibited severe deficiency in the formation of intercellular nanotubes (Figures 1Ca, 1Cb, and 1D). Consistently, the mutant was blocked in generating extending nanotubes (Figure S1A), shown to be produced at low cell density (Dubey et al., 2016). Ectopic complementation of the mutant with *CORE* genes restored nanotube formation to that of wild-type levels (Figures 1Cc and 1D). Importantly, nanotube structures were readily evident in bacteria deleted of genes encoding non-*CORE* key flagellar components. These include mutants lacking *hag*, encoding flagellin; *flgB*, *flgC*, *fliE*, and *fliF* (*ΔflgB–fliF*), encoding non-*CORE* basal body components; and *fliI*, encoding the flagellar ATPase, a key component of the CORE-associated sorting platform (Figures 1B, 1Cj, 1D, and S1B) (Minamino and Imada, 2015). These results indicate that the defect observed in nanotube production can be directly attributed to the function of the *CORE*, suggesting a dual function for this complex in biogenesis of either flagella or nanotubes.

To elucidate whether all six *CORE* genes are required for nanotube projection, we deleted each gene individually. Strains lacking *fliO*, *fliP*, *fliQ*, or *flhA* were severely deficient in nanotube construction, whereas *flhB* mutant could seldom form nanotubes, but these were very slim and frequently torn apart (Figures 1Cd–1Ci and 1D). Interestingly, *fliR* mutant generated very short projections, exhibiting a bristle-like shape (Figure 1Cg), suggesting that nanotube formation was initiated but their elongation process was halted. Reintroducing each *CORE* gene into the corresponding *CORE* mutant restored nanotube development (Figures S1C and S1D). Thus, all CORE components are required for production of proper nanotubes, though lack of each component affects the process with slight variations, highlighting further complexity layer in nanotube generation.

CORE-F_{Bs} Is Required for Intercellular Molecular Trade

Having established that the *CORE* genes are required for nanotube development, we next sought to explore their influence on intercellular molecular exchange. Previously, we found that mixing two strains, each harboring a different antibiotic resistance gene, results in the exchange of antibiotic resistance enzymes in a nanotube-dependent path, yielding a population of cells transiently resistant to both antibiotics (protein exchange). Furthermore, in a similar manner, we detected the delivery of a non-conjugative plasmid from donor to recipient (plasmid exchange) (Dubey and Ben-Yehuda, 2011). Indeed, a *Bs* mutant lacking the *CORE* genes was severely deficient in both protein and plasmid exchange (Figure 2). Consistently, both defects were cured by reintroducing the *CORE* genes into the mutant strain (Figure 2). Analyzing the *CORE* single mutants revealed that they were all significantly impaired in protein exchange, with Δ*flhA* and Δ*flhB* showing the most severe phenotype, whereas *fliR* mutant, harboring the bristle-like nanotubes, was the least affected (Figures 1Cg and 2). Moreover, each and every single mutant was fully defective in plasmid exchange (Figure 2), indicating that such event exemplifies a more challenging task than protein trade. Importantly, none of the *CORE* mutants exhibited any measurable growth defect (Figures S1E and S1F). The capacity to exchange proteins and plasmids was regained by complementing the individual *CORE* mutants with the corresponding *CORE* gene (Figure S2A). Mutants lacking non-*CORE* flagellum genes (*flgB–fliF*, *fliI*, and *hag*) were capable of performing molecular exchange, while their motility was fully blocked (Figure 2). Notably, Δ*flgB–fliF* and Δ*fliI* strains exhibited minor deficiency in both protein and plasmid exchange that is consistent with the modestly reduced number of nanotube structures detected (Figures 1D and 2). Because the expression of *CORE* genes was not perturbed by these mutations (Figure S1G), this effect might imply some role of these proteins in stabilizing the CORE complex. Overall, our results strengthen the view that the CORE-F_{Bs} mediates intercellular molecular trafficking via nanotubes.

Next, we examined the impact of CORE on nanotube-dependent interspecies interactions. We have previously shown that *Bs* kills neighboring *B. megaterium* (*Bm*) cells by delivering the tRNase toxin WapA via nanotubes (Stempler et al., 2017). GFP-labeled *Bs* was mixed with *Bm*, and cells were visualized using time-lapse microscopy. *Bs* cells, lacking *CORE*, indeed failed to arrest *Bm* growth and division, inferring that the transfer of WapA toxin into *Bm* cells was impeded (Figure S2B). Consistently, ectopic expression of *CORE* genes restored this capability (Figure S2B). Thus, interspecies delivery of WapA via nanotubes is CORE dependent.

CORE Components Are Localized to the Site of Nanotube Emergence

Since the CORE complex is a prime constituent of the flagellar basal body (Diepold and Wagner, 2014), we posited that in a similar fashion, the CORE forms a platform from which nanotubes emerge and extend. The major CORE component FlhA,

(C) The indicated *Bs CORE* mutant strains were visualized using XHR-SEM to monitor the formation of intercellular nanotubes. Strains were grown to the mid-logarithmic phase, spotted onto EM grids, incubated on LB agar plates for 4 h at 37°C, and visualized using XHR-SEM. Scale bar represents 500 nm.
(D) Quantification of the average number of nanotubes displayed per 50 cells by the indicated *Bs* mutant strains following XHR-SEM analysis described in (C). Shown are average values and SD of at least three independent experiments ($n \geq 200$ for each strain).
See also Figure S1.

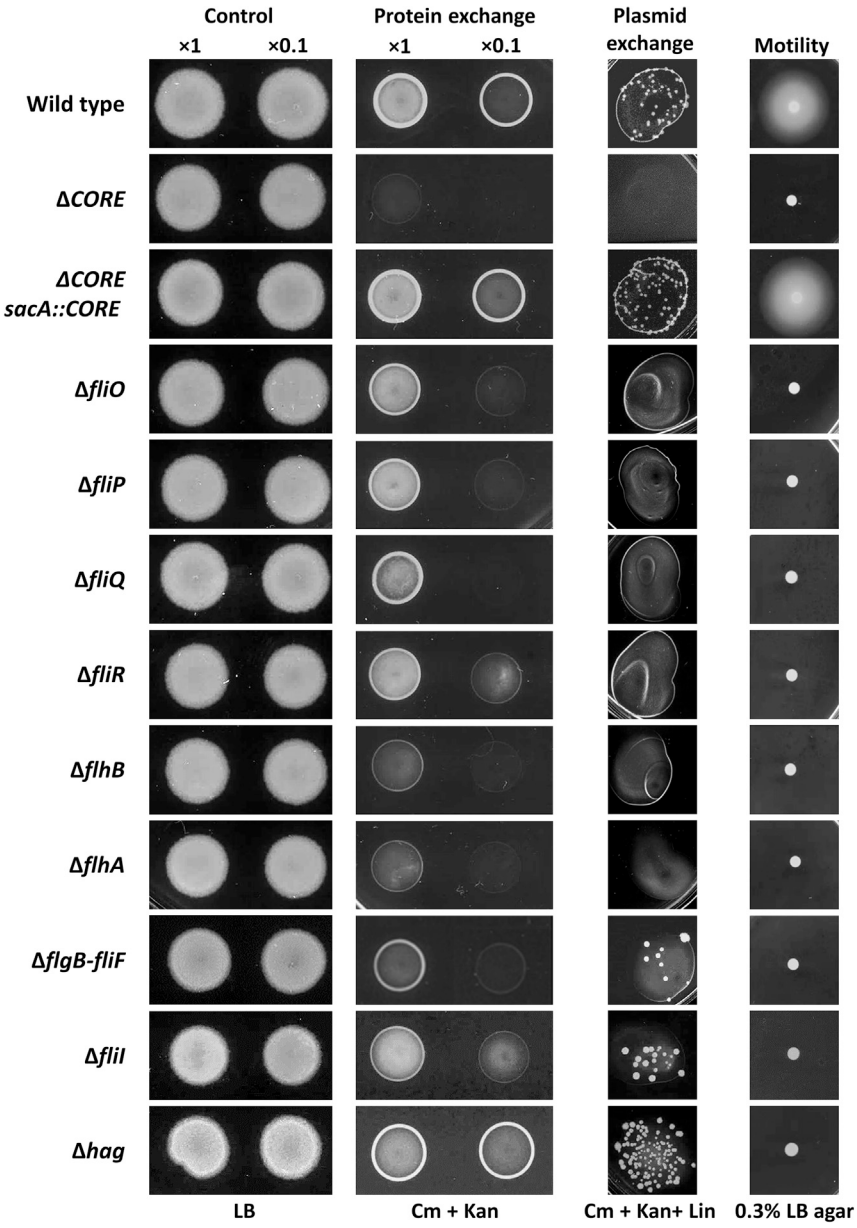

Figure 2. *Bs CORE* Mutants Are Deficient in Molecular Exchange

Assessing molecular exchange in *CORE* mutants. For protein exchange assay, pairs of a donor (SB463: *amyE*::$P_{hyper\text{-}spank}$-*cat-spec*) (Cm^R, $Spec^R$) and a recipient (SB513: *amyE*::$P_{hyper\text{-}spank}$-*gfp-kan*) (Kan^R) parental strains (wild-type) were used. The investigated mutants harbor the corresponding genotypes and carry the indicated null mutation in both donor and recipient strains. Donor and recipient strains were mixed in 1:1 ratio (at two concentrations, 1× and 0.1×) and incubated in LB supplemented with 1 mM IPTG for 4 h at 37°C with gentle shaking. Equal numbers of cells were then spotted onto LB agar (control) and LB agar containing chloramphenicol (Cm) and kanamycin (Kan) (protein exchange) and photographed after 18 h. For plasmid exchange assay, pairs of a donor (GD110: *amyE*::$P_{hyper\text{-}spank}$-*cat-spec*, pHB201/*cat*, *erm*) (Cm^R, $Spec^R$, Mls^R) and a recipient (SB513: *amyE*::$P_{hyper\text{-}spank}$-*gfp-kan*) (Kan^R) parental strains (wild-type) were used, with the investigated mutants harbor in addition the indicated null mutation in both donor and recipient strains. Cells were mixed in 1:1 ratio (concentration 1×), processed as described for protein exchange, and spotted onto LB agar containing Cm, Kan, and lincomycin (Lin) (plasmid exchange). Cells were incubated at 37°C, and colonies were photographed after 36 h of incubation. For motility assay, wild-type (PY79) and the indicated mutant strains were grown to the mid-logarithmic phase and spotted onto LB plates containing 0.3% agar and photographed after 7 h of incubation at 37°C (motility). See also Figures S1 and S2.

harboring a large cytoplasmic domain (Figure 1A) (Morimoto et al., 2014), was fused to GFP. The fusion rendered the protein partially functional (Figures S3A–S3C); however, the few nanotubes produced by these cells emerged from sites adjacent to FlhA-GFP focal assemblies (Figures S3D and S3E), hinting that nanotubes are projected from CORE-containing complexes. To further establish this notion, we co-visualized nanotubes and CORE components at high resolution by using immuno-XHR-SEM. To this end, FliP was HA-tagged in its C terminus, predicted to be exposed at the cell surface (Fukumura et al., 2017) (Figure 1A), and introduced into the *Bs* genome ectopically. Next, cells were subjected to immuno-XHR-SEM, using primary anti-HA antibody followed by gold-labeled secondary antibodies. Strikingly, a gold particle was recurrently observed at the site of nanotube emanation, signifying that indeed the CORE serves as the basal body for nanotube construction (Figures 3A and 3B). Consistently, signal from FliP was also detected at the origin of extending nanotubes (Figure S4A). Tagging FliP at a site predicted to form a surface-exposed loop (Fukumura et al., 2017) showed a similar outcome (Figure S4B). Furthermore, use of a mutant (*Δmbl*) exhibiting a defect in cell wall assembly (Jones et al., 2001) to improve antibody accessibility to CORE complexes, or a strain harboring tagged *fliP* as a sole copy, yielded a similar gold labeling pattern (Figures 3C, 3D, and S4C). Significantly, in all viewed cases (25), the signal from FliP was restricted to only one end of a connecting nanotube, suggesting that the CORE is exploited for nanotube projection by the producing cell, while docking on a recipient cell is CORE independent. Of note, detection of only a single gold particle (18 nm) associated with the FliP multimeric ring (10 nm in diameter; Fukumura et al., 2017; Kuhlen et al., 2018) is most likely due to resolution limit or steric hindrance. As a control, no gold signal was obtained from cells lacking the HA tagged protein (Figure S4D) or from cells expressing a membrane protein tagged at a site facing the cytoplasm (Figures S4E and S4F) (Rudner

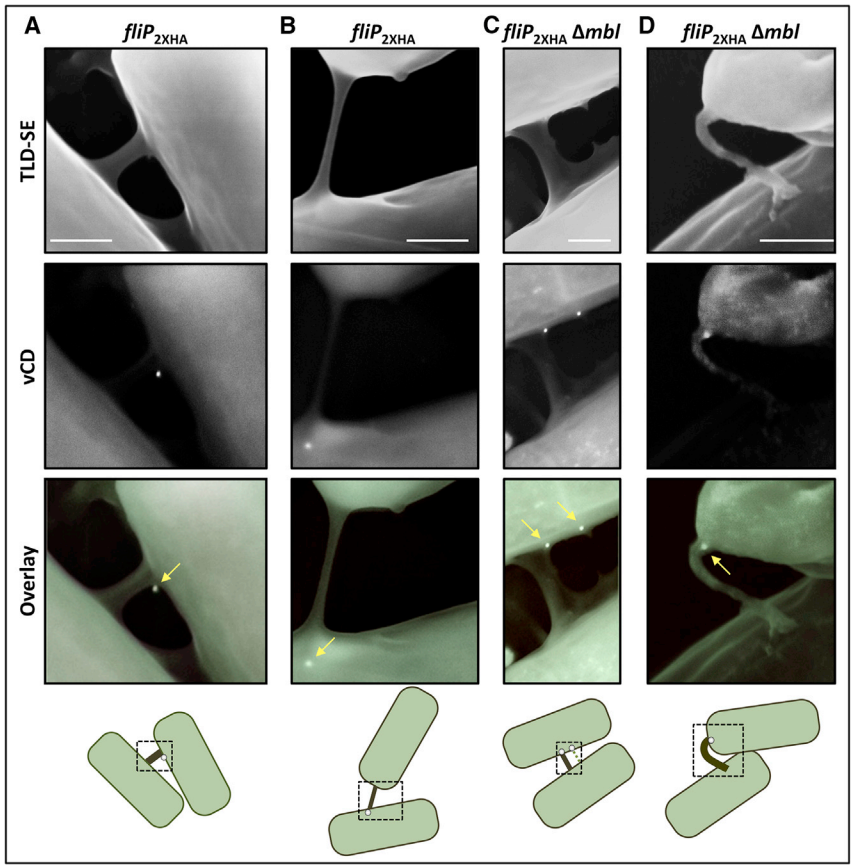

Figure 3. FliP Localizes to the Base of Nanotubes

Cells expressing HA-tagged FliP (SH93: *amyE*::$P_{hyper\text{-}spank}$-*fliP*$_{2xHA}$, *sacA*::$P_{hyper\text{-}spank}$-*ymdB*, A and B, or SH110: *amyE*::$P_{hyper\text{-}spank}$-*fliP*$_{2xHA}$, *sacA*::$P_{hyper\text{-}spank}$-*ymdB, Δmbl*, C and D) were spotted onto EM grids and subjected to immuno-gold XHR-SEM, using primary antibodies against HA and secondary gold-conjugated antibodies. Samples were not coated before observation. Examples of $FliP_{2xHA}$ localization (white dots) at the base of nanotubes are presented (indicated by arrows). Shown are XHR-SEM images that were acquired using TLD-SE (through-lens detector-secondary electron) for nanotubes visualization and vCD (low-kV high-contrast backscattered detector) for gold particle detection, as well as overlay of both images. Schematic below depicts the interpretive cell layout and highlights the nanotube region with gold signal (dashed box) captured by XHR-SEM. Scale bars represent 200 nm. See also Figures S3 and S4.

et al., 2002). Furthermore, cells harboring a surface-exposed tag in an unrelated membrane protein yielded a scattered pattern, which did not coincide with nanotube emanation sites (Tzipilevich et al., 2017) (Figures S4G and S4H). Hence, we conclude that the CORE provides a platform for nanotube emergence.

Flagellar CORE Complexes Are Used for Nanotube Formation by Diverse Species

On the basis of our results, we asked whether the flagellar CORE of other bacterial species is bi-functional and similarly to CORE-F_{Bs} can give rise to both flagella and nanotubes. We thus deleted the *CORE* genes from the genomes of *Bm*, a close relative of *Bs*, the Gram-positive human pathogen *Listeria monocytogenes* (*Lm*), and the evolutionary distant *Escherichia coli* (*Ec*) (Table S1). Wild-type, Δ*CORE*, and mutants lacking the flagellum filament (Δ*flagellin*) from all tested species were incubated on a solid surface to induce nanotube formation and subsequently examined using XHR-SEM. While nanotube appendages were plentiful in wild-type and in strains devoid of flagellum filaments, they were absent from the corresponding *CORE* mutants (Figure 4A), hence corroborating that the flagellar CORE is used by diverse species for nanotube production.

We then investigated the cross-species functional conservation of COREs by testing the capacity of foreign flagellar CORE complexes to complement nanotube formation by *CORE* deficient *Bs*. Introducing *CORE*-F_{Bm} genes into *Bs* Δ*CORE* mutant prompted the formation of intercellular nanotubular structures to a level close to that of wild-type *Bs* (Figures 4B and 4C). Compellingly, also *CORE*-F_{Lm} and *CORE*-F_{Ec} genes induced the formation of nanotubes in *Bs* Δ*CORE*, although of an apparent thin morphology (Figures 4B and 4C). Interestingly, however, motility was reestablished by *CORE*-F_{Bm} but could not be restored by *CORE*-F_{Lm} or *CORE*-F_{Ec} (Figure 4D). Consistent with the complete restoration of nanotubes by *CORE*-F_{Bm}, both protein and plasmid exchange levels were regained to levels comparable with that of wild-type *Bs* (Figure 4D). In line with the limited nanotube restitution (Figure 4C), *CORE*-F_{Lm} and *CORE*-F_{Ec} enabled partial protein exchange but could not support plasmid exchange (Figure 4D), indicating that additional non-CORE components that differ among species are involved in this process. Taken together, our results suggest that distinct bacterial species carrying flagellar *CORE* genes have the potential to form nanotubes.

CORE Complexes Are Universal and Phylogenetically Widespread

We next addressed the ubiquity of the *CORE* genes across the bacterial kingdom. Since previous such analyses included primarily genomes of Gram-negative bacteria (Abby and Rocha, 2012; Hu et al., 2017; Snyder et al., 2009), here we attempted to include representatives of the majority of the bacterial phyla. Using the STRING database homology data (Szklarczyk et al., 2017; von Mering et al., 2007), we analyzed 400 species belonging to 18 phyla. We found *CORE* genes to be widespread in all the examined bacterial phyla, typically as part of the flagellum or its homologous injectisome apparatus (Figure S5; Table S2). Interestingly, some bacteria lacking a substantial fraction of the gene cohort required for formation of these organelles still harbor the *CORE* genes that could function to nucleate

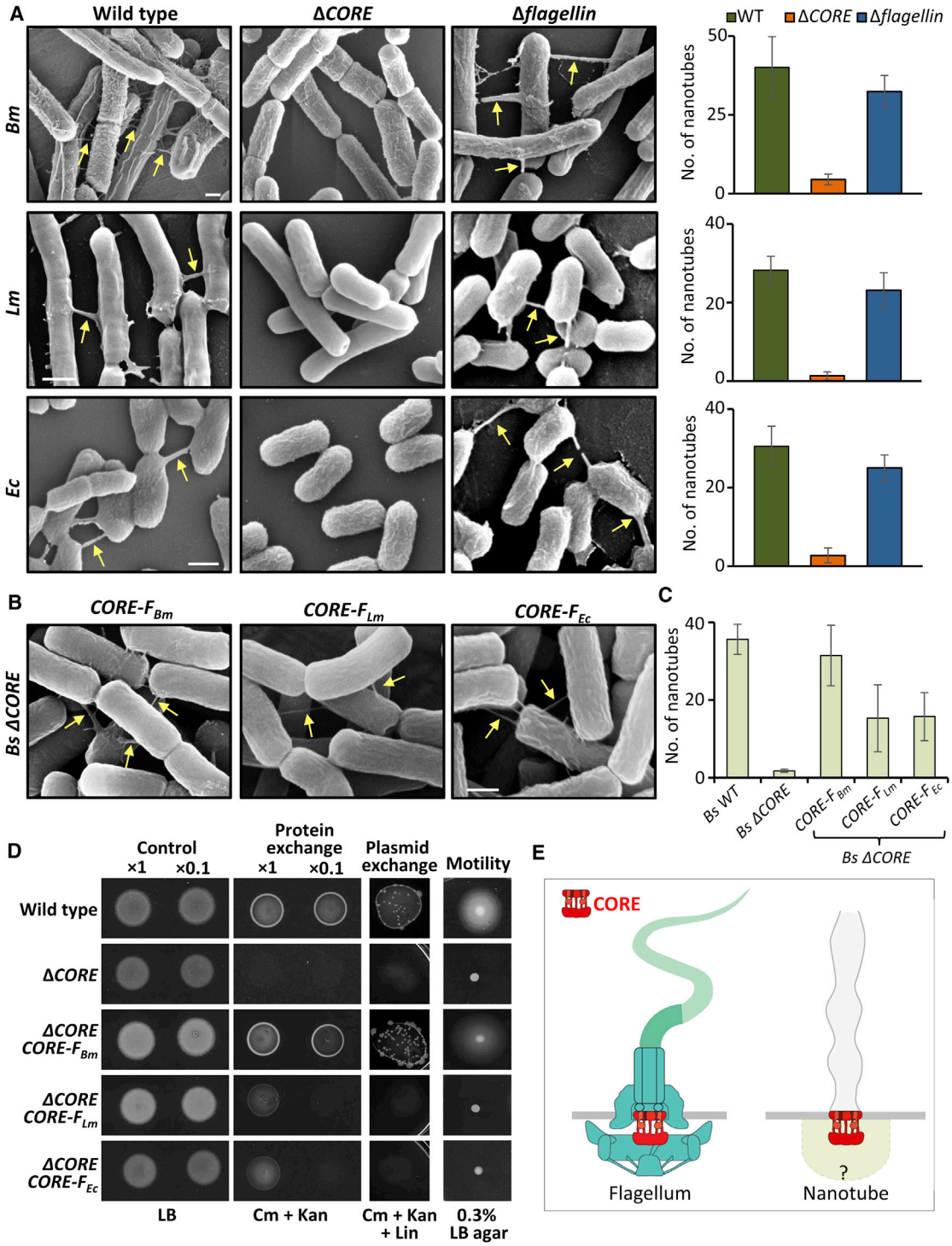

Figure 4. CORE Is a Widespread Complex with Conserved Functions across Species

(A) Wild-type *Bm* (OS2), *Lm* (10403S), and *Ec* (MG1655) and their corresponding mutant strains lacking *CORE* (*ΔCORE*) or gene encoding flagellin (*Δflagellin*) were grown to the mid-logarithmic phase, spotted onto EM grids followed by incubation on LB agar plates for 4 h at 37°C, and visualized using XHR-SEM. Arrows indicate nanotubes. Scale bar represents 500 nm. Right: quantification of the average number of nanotubes displayed per 50 cells by the indicated strains following XHR-SEM analysis. Shown are average values and SD of at least three independent experiments ($n \geq 200$ for each strain).

(B) Cells of *Bs* (Δ*CORE*) complemented with *Bm* flagellar *CORE* (*CORE-F*$_{Bm}$), *Lm* flagellar *CORE* (*CORE-F*$_{Lm}$), and *Ec* flagellar *CORE* (*CORE-F*$_{Ec}$) were processed as in (A) and visualized using XHR-SEM. Arrows indicate nanotubes. Scale bar represents 500 nm.

(legend continued on next page)

exclusively nanotube biogenesis. These bacteria include *Myxococci* species (phylum Proteobacteria), *Chloracidobacterium thermophilum* (phylum Acidobacteria), and *Succinatimonas hippie* (phylum Proteobacteria) (Figure S5; Table S2) (Abby and Rocha, 2012; Hu et al., 2017). Overall, this examination emphasizes that a wide spectrum of species possesses the potential to produce nanotubes and use them for molecular exchange.

DISCUSSION

We uncovered that the export apparatus of the flagella, designated CORE, is a dual-functional complex, communally serving as a foundation for both flagella and nanotube generation (Figure 4E). This complex is likely to promote flagella formation by planktonic bacteria but alternates to support nanotube formation by bacteria grown on solid surfaces. The functional conservation of CORE complexes from distinct bacterial species was revealed by their ability to support nanotube formation in *Bs* mutant lacking endogenous *CORE* genes. Our findings insinuate that CORE-dependent molecular trafficking among bacteria is extensive and broad and includes a large array of cytoplasmic molecules. As such, it fundamentally expands the bacterial metabolic flexibility, facilitating the acquisition of new features. Furthermore, the observation that even plasmid trafficking uses CORE-dependent nanotubes highlights the potential impact of CORE complexes on horizontal gene transfer in nature. In the accompanying study, we discovered a similar set of highly conserved injectisome CORE proteins in EPEC to be implicated in extraction of cytoplasmic molecules from infected human host cells via nanotubes (Pal et al., 2019). On the basis of our findings, we postulate that the CORE represents an evolutionary ancestral functional unit, which subsequently evolved by acquisition of additional components, into nanotube, flagellum, or injectisome.

Some bacteria, including *Vibrio cholerae* and *Helicobacter pylori*, form flagella encased by membranous protrusions, termed "sheathed flagella." Intriguingly, these bacteria were reported to occasionally produce "empty sheaths," with a structure highly resembling nanotubes (Allen and Baumann, 1971; Geis et al., 1993; McCarter, 2001). Furthermore, the existence of isolated orphan CORE components in various bacterial genomes, frequently referred to as truncated or incomplete systems (Pallen and Matzke, 2006; Ren et al., 2005), insinuates their potential nanotube designation.

The discovery that CORE serves as a platform for nanotube biogenesis could provide the foundation for elucidating central aspects of nanotube functionality, such as the selection of the delivered molecular cargo, the source of energy used for cargo transportation, the directionality of nanotube operation, and the fusion mechanism with recipient cell membrane. Further mechanistic insight into nanotube biogenesis and function may escort the development of innovative methodologies, enabling control of intercellular molecular trade among bacteria, to attain intelligent bacterial community design.

STAR★METHODS

Detailed methods are provided in the online version of this paper and include the following:

- KEY RESOURCES TABLE
- CONTACT FOR REAGENT AND RESOURCE SHARING
- EXPERIMENTAL MODEL AND SUBJECT DETAILS
  - Details on bacterial strain construction
- METHOD DETAILS
  - General growth conditions
  - Details on plasmid construction
  - Nanotube visualization by XHR-SEM
  - Immuno-XHR-SEM analysis
  - Molecular exchange assay
  - Motility assay
  - Fluorescence microscopy
  - RNA isolation and qRT-PCR
  - Phylogenetic analysis
- QUANTIFICATION AND STATISTICAL ANALYSIS

SUPPLEMENTAL INFORMATION

Supplemental Information can be found with this article online at https://doi.org/10.1016/j.celrep.2019.02.055.

ACKNOWLEDGMENTS

We thank E. Blayvas and A. Ben-Hur (Hebrew University) for help with XHR-SEM and R. Nir-Paz (Hadassah Hospital) and A. Herskovits (Tel Aviv University)

(C) Quantification of the average number of nanotubes displayed per 50 cells by the indicated strains following XHR-SEM analysis described in (B). Shown are average values and SD of at least three independent experiments ($n \geq 200$ for each strain).
(D) Assessing molecular exchange in *Bs* Δ*CORE* strain complemented with exogenous *CORE* genes. For protein exchange assay, pairs of a donor (SB463: *amyE*::$P_{hyper\text{-}spank}$-*cat-spec*) (Cm^R, $Spec^R$) and a recipient (SB513: *amyE*::$P_{hyper\text{-}spank}$-*gfp-kan*) (Kan^R) parental strains (wild-type) were used. The investigated strains *ΔCORE* and *ΔCORE* complemented with *CORE-*F_{Bm}, *CORE-*F_{Lm}, and *CORE-*F_{Ec} (controlled by *Bs* $P_{fla/che}$ promoter) harbor the corresponding genotypes of donor and recipient. Donor and recipient strains were mixed in 1:1 ratio (at two concentrations, 1× and 0.1×) and incubated in LB supplemented with 1 mM IPTG for 4 h at 37°C with gentle shaking. Equal numbers of cells were then spotted onto LB agar (control) and LB agar containing chloramphenicol (Cm) and kanamycin (Kan) (protein exchange) and photographed after 18 h. For plasmid exchange assay, pairs of a donor (GD110: *amyE*::$P_{hyper\text{-}spank}$-*cat-spec*, pHB201/*cat*, *erm*) (Cm^R, $Spec^R$, Mls^R) and a recipient (SB513: *amyE*::$P_{hyper\text{-}spank}$-*gfp-kan*) (Kan^R) parental strains (wild-type) were used. The investigated strains complemented with exogenous *CORE*s harbor the corresponding genotypes of donor and recipient strains. Cells were mixed in 1:1 ratio (concentration 1×), processed as described for protein exchange, and spotted onto LB agar containing Cm, Kan, and lincomycin (Lin) (plasmid exchange). Cells were incubated at 37°C, and colonies were photographed after 36 h of incubation. For motility assay, wild-type (PY79) and the indicated strains were grown to mid-logarithmic phase, spotted onto LB plates containing 0.3% agar, and photographed after 7 h of incubation at 37°C (motility).
(E) A schematic model depicting the modularity of CORE complexes in flagellum and nanotube. CORE-associated components of the nanotube basal body are missing. Flagellum structure was adapted from (Dietsche et al., 2016).
See also Figure S5 and Tables S1 and S2.

for strains and plasmids. We are grateful to S. Wagner (Tubingen University) for help generating Figure 4E and valuable insight. We are indebted to A. Rouvinski (Hebrew University) and members of the Ben-Yehuda and Rosenshine laboratories for valuable discussions. This work was supported by a European Research Council Advance grant (339984) awarded to S.B.-Y.; a grant from the Israel Science Foundation (617/15) awarded to I.R.; a European Research Council Synergy grant (810186) awarded to S.B.-Y. and I.R.; and a grant from the Israel Science Foundation (876/17) awarded to H.M. S.B. is partially funded by the Lady Davis Fellowship Trust, and Y.E.G. is partially supported by the Hoffman Program.

AUTHOR CONTRIBUTIONS

S.B., A.K.B., R.R.P., G.M., and Y.E.G. performed the experiments. S.B., A.K.B., R.R.P., Y.E.G., H.M., S.B.-Y., and I.R. conceived the experiments and analyzed the data. S.B., A.K.B., R.R.P., S.B.-Y., and I.R. wrote the manuscript. S.B.-Y. and I.R. managed the project.

DECLARATION OF INTERESTS

The authors declare no competing interests.

Received: May 8, 2018
Revised: February 5, 2019
Accepted: February 13, 2019
Published: March 28, 2019

REFERENCES

Abby, S.S., and Rocha, E.P. (2012). The non-flagellar type III secretion system evolved from the bacterial flagellum and diversified into host-cell adapted systems. PLoS Genet. *8*, e1002983.

Allen, R.D., and Baumann, P. (1971). Structure and arrangement of flagella in species of the genus *Beneckea* and *Photobacterium fischeri*. J. Bacteriol. *107*, 295–302.

Argov, T., Rabinovich, L., Sigal, N., and Herskovits, A.A. (2017). An effective counterselection system for *Listeria monocytogenes* and its use to characterize the monocin genomic region of strain 10403S. Appl. Environ. Microbiol. *83*, e02927-16.

Baidya, A.K., Bhattacharya, S., Dubey, G.P., Mamou, G., and Ben-Yehuda, S. (2018). Bacterial nanotubes: a conduit for intercellular molecular trade. Curr. Opin. Microbiol. *42*, 1–6.

Bejerano-Sagie, M., Oppenheimer-Shaanan, Y., Berlatzky, I., Rouvinski, A., Meyerovich, M., and Ben-Yehuda, S. (2006). A checkpoint protein that scans the chromosome for damage at the start of sporulation in *Bacillus subtilis*. Cell *125*, 679–690.

Benomar, S., Ranava, D., Cárdenas, M.L., Trably, E., Rafrafi, Y., Ducret, A., Hamelin, J., Lojou, E., Steyer, J.P., and Giudici-Orticoni, M.T. (2015). Nutritional stress induces exchange of cell material and energetic coupling between bacterial species. Nat. Commun. *6*, 6283.

Bron, S., Bolhuis, A., Tjalsma, H., Holsappel, S., Venema, G., and van Dijl, J.M. (1998). Protein secretion and possible roles for multiple signal peptidases for precursor processing in bacilli. J. Biotechnol. *64*, 3–13.

Costa, T.R., Felisberto-Rodrigues, C., Meir, A., Prevost, M.S., Redzej, A., Trokter, M., and Waksman, G. (2015). Secretion systems in Gram-negative bacteria: structural and mechanistic insights. Nat. Rev. Microbiol. *13*, 343–359.

Datsenko, K.A., and Wanner, B.L. (2000). One-step inactivation of chromosomal genes in *Escherichia coli* K-12 using PCR products. Proc. Natl. Acad. Sci. U S A *97*, 6640–6645.

Diepold, A., and Armitage, J.P. (2015). Type III secretion systems: the bacterial flagellum and the injectisome. Philos. Trans. R. Soc. Lond. B Biol. Sci. *370*, 20150020.

Diepold, A., and Wagner, S. (2014). Assembly of the bacterial type III secretion machinery. FEMS Microbiol. Rev. *38*, 802–822.

Dietsche, T., Tesfazgi Mebrhatu, M., Brunner, M.J., Abrusci, P., Yan, J., Franz-Wachtel, M., Schärfe, C., Zilkenat, S., Grin, I., Galán, J.E., et al. (2016). Structural and functional characterization of the bacterial type III secretion export apparatus. PLoS Pathog. *12*, e1006071.

Dubey, G.P., and Ben-Yehuda, S. (2011). Intercellular nanotubes mediate bacterial communication. Cell *144*, 590–600.

Dubey, G.P., Malli Mohan, G.B., Dubrovsky, A., Amen, T., Tsipshtein, S., Rouvinski, A., Rosenberg, A., Kaganovich, D., Sherman, E., Medalia, O., and Ben-Yehuda, S. (2016). Architecture and characteristics of bacterial nanotubes. Dev. Cell *36*, 453–461.

Fabiani, F.D., Renault, T.T., Peters, B., Dietsche, T., Gálvez, E.J.C., Guse, A., Freier, K., Charpentier, E., Strowig, T., Franz-Wachtel, M., et al. (2017). A flagellum-specific chaperone facilitates assembly of the core type III export apparatus of the bacterial flagellum. PLoS Biol. *15*, e2002267.

Fukumura, T., Makino, F., Dietsche, T., Kinoshita, M., Kato, T., Wagner, S., Namba, K., Imada, K., and Minamino, T. (2017). Assembly and stoichiometry of the core structure of the bacterial flagellar type III export gate complex. PLoS Biol. *15*, e2002281.

Geis, G., Suerbaum, S., Forsthoff, B., Leying, H., and Opferkuch, W. (1993). Ultrastructure and biochemical studies of the flagellar sheath of *Helicobacter pylori*. J. Med. Microbiol. *38*, 371–377.

Gibson, D.G. (2011). Enzymatic assembly of overlapping DNA fragments. Methods Enzymol. *498*, 349–361.

Guérout-Fleury, A.M., Frandsen, N., and Stragier, P. (1996). Plasmids for ectopic integration in *Bacillus subtilis*. Gene *180*, 57–61.

Harwood, C.R., and Cutting, S.M. (1990). Molecular biological methods for *Bacillus* (Wiley).

Hayes, C.S., Aoki, S.K., and Low, D.A. (2010). Bacterial contact-dependent delivery systems. Annu. Rev. Genet. *44*, 71–90.

Hu, Y., Huang, H., Cheng, X., Shu, X., White, A.P., Stavrinides, J., Köster, W., Zhu, G., Zhao, Z., and Wang, Y. (2017). A global survey of bacterial type III secretion systems and their effectors. Environ. Microbiol. *19*, 3879–3895.

Hueck, C.J. (1998). Type III protein secretion systems in bacterial pathogens of animals and plants. Microbiol. Mol. Biol. Rev. *62*, 379–433.

Jones, L.J., Carballido-López, R., and Errington, J. (2001). Control of cell shape in bacteria: helical, actin-like filaments in *Bacillus subtilis*. Cell *104*, 913–922.

Kearns, D.B., and Losick, R. (2003). Swarming motility in undomesticated *Bacillus subtilis*. Mol. Microbiol. *49*, 581–590.

Kuhlen, L., Abrusci, P., Johnson, S., Gault, J., Deme, J., Caesar, J., Dietsche, T., Mebrhatu, M.T., Ganief, T., Macek, B., et al. (2018). Structure of the core of the type III secretion system export apparatus. Nat. Struct. Mol. Biol. *25*, 583–590.

Lemon, K.P., and Grossman, A.D. (1998). Localization of bacterial DNA polymerase: evidence for a factory model of replication. Science *282*, 1516–1519.

Li, X.T., Thomason, L.C., Sawitzke, J.A., Costantino, N., and Court, D.L. (2013). Positive and negative selection using the *tetA-sacB* cassette: recombineering and P1 transduction in *Escherichia coli*. Nucleic Acids Res. *41*, e204.

McCaig, W.D., Koller, A., and Thanassi, D.G. (2013). Production of outer membrane vesicles and outer membrane tubes by *Francisella novicida*. J. Bacteriol. *195*, 1120–1132.

McCarter, L.L. (2001). Polar flagellar motility of the *Vibrionaceae*. Microbiol. Mol. Biol. Rev. *65*, 445–462.

Minamino, T., and Imada, K. (2015). The bacterial flagellar motor and its structural diversity. Trends Microbiol. *23*, 267–274.

Morimoto, Y.V., Ito, M., Hiraoka, K.D., Che, Y.S., Bai, F., Kami-Ike, N., Namba, K., and Minamino, T. (2014). Assembly and stoichiometry of FliF and FlhA in *Salmonella* flagellar basal body. Mol. Microbiol. *91*, 1214–1226.

Moro, A., Sanchez, J.C., and Serguera, C. (1995). Transformation of *Bacillus megaterium* by electroporation. Biotechnol. Tech. *9*, 589–590.

Pal, R.R., Baidya, A.K., Mamou, G., Bhattacharya, S., Socol, Y., Kobi, S., Katsowich, N., Ben-Yehuda, S., and Rosenshine, I. (2019). Pathogenic

E. coli extracts nutrients from infected host cells utilizing injectisome components. Cell *177*, Published online March 28, 2019. https://doi.org/10.1016/j.cell.2019.02.022.

Pallen, M.J., and Matzke, N.J. (2006). From The Origin of Species to the origin of bacterial flagella. Nat. Rev. Microbiol. *4*, 784–790.

Pande, S., Shitut, S., Freund, L., Westermann, M., Bertels, F., Colesie, C., Bischofs, I.B., and Kost, C. (2015). Metabolic cross-feeding via intercellular nanotubes among bacteria. Nat. Commun. *6*, 6238.

Ren, C.P., Beatson, S.A., Parkhill, J., and Pallen, M.J. (2005). The Flag-2 locus, an ancestral gene cluster, is potentially associated with a novel flagellar system from *Escherichia coli*. J. Bacteriol. *187*, 1430–1440.

Rosenberg, A., Sinai, L., Smith, Y., and Ben-Yehuda, S. (2012). Dynamic expression of the translational machinery during *Bacillus subtilis* life cycle at a single cell level. PLoS ONE *7*, e41921.

Rudner, D.Z., Pan, Q., and Losick, R.M. (2002). Evidence that subcellular localization of a bacterial membrane protein is achieved by diffusion and capture. Proc. Natl. Acad. Sci. U S A *99*, 8701–8706.

Snyder, L.A., Loman, N.J., Fütterer, K., and Pallen, M.J. (2009). Bacterial flagellar diversity and evolution: seek simplicity and distrust it? Trends Microbiol. *17*, 1–5.

Stempler, O., Baidya, A.K., Bhattacharya, S., Malli Mohan, G.B., Tzipilevich, E., Sinai, L., Mamou, G., and Ben-Yehuda, S. (2017). Interspecies nutrient extraction and toxin delivery between bacteria. Nat. Commun. *8*, 315.

Szklarczyk, D., Morris, J.H., Cook, H., Kuhn, M., Wyder, S., Simonovic, M., Santos, A., Doncheva, N.T., Roth, A., Bork, P., et al. (2017). The STRING database in 2017: quality-controlled protein-protein association networks, made broadly accessible. Nucleic Acids Res. *45* (*D1*), D362–D368.

Thomason, L.C., Costantino, N., and Court, D.L. (2007). E. coli genome manipulation by P1 transduction. Curr. Protoc. Mol. Biol. *Chapter 1*, Unit 1.17.

Tzipilevich, E., Habusha, M., and Ben-Yehuda, S. (2017). Acquisition of phage sensitivity by bacteria through exchange of phage receptors. Cell *168*, 186–199.e12.

von Mering, C., Jensen, L.J., Kuhn, M., Chaffron, S., Doerks, T., Krüger, B., Snel, B., and Bork, P. (2007). STRING 7—recent developments in the integration and prediction of protein interactions. Nucleic Acids Res. *35*, D358–D362.

Wei, X., Vassallo, C.N., Pathak, D.T., and Wall, D. (2014). *Myxobacteria* produce outer membrane-enclosed tubes in unstructured environments. J. Bacteriol. *196*, 1807–1814.

Youngman, P., Perkins, J.B., and Losick, R. (1984). Construction of a cloning site near one end of Tn917 into which foreign DNA may be inserted without affecting transposition in *Bacillus subtilis* or expression of the transposon-borne *erm* gene. Plasmid *12*, 1–9.

Yu, D., Ellis, H.M., Lee, E.C., Jenkins, N.A., Copeland, N.G., and Court, D.L. (2000). An efficient recombination system for chromosome engineering in *Escherichia coli*. Proc. Natl. Acad. Sci. U S A *97*, 5978–5983.

STAR★METHODS

KEY RESOURCES TABLE

REAGENT or RESOURCE	SOURCE	IDENTIFIER
Antibodies		
Polyclonal anti-HA antibodies (Rabbit)	Thermo Fisher Scientific	Cat#:71-5500; RRID: AB_2533988
Polyclonal anti-GFP antibodies (Rabbit)	Laboratory stock (Dubey and Ben-Yehuda, 2011)	NA
18 nm gold-conjugated IgG secondary antibody Goat anti-Rabbit.	Jackson ImmunoResearch Laboratories	Cat#: 111-215-144; RRID: AB_2338017
Chemicals, Peptides, and Recombinant Proteins		
Chloramphenicol	Sigma-Aldrich	Cat#: C0378
Tetracycline	Sigma-Aldrich	Cat#: 87128
Kanamycin	US Biological	Cat#: K0010
Lincomycin	Sigma-Aldrich	Cat#: 62143-5G
Erythromycin	Sigma-Aldrich	Cat#: E0774
Spectinomycin	Sigma-Aldrich	Cat#: S4014-5G
Ampicillin	Sigma-Aldrich	Cat#: A9518-25G
IPTG (Isopropyl β-D-1-thiogalactopyranoside)	Sigma-Aldrich	Cat#: I6758-5G
D-Xylose	Sigma-Aldrich	Cat#: X1500-1KG
Sucrose	J.T.Baker	Cat#: 4072-05
Polyethylene glycol 8000	Promega	Cat#: V3011
D-Sorbitol	Sigma-Aldrich	Cat#: S6021
Paraformaldehyde	Electron Microscopy Sciences	Cat#: 15710
Glutaraldehyde	Electron Microscopy Sciences	Cat#: 16020
Sodium Cacodylate Buffer (pH 7.4)	Electron Microscopy Sciences	Cat#: 11650
FM4-64	Molecular probes/ Thermo Fisher Scientific	Cat#: T13320
Critical Commercial Assays		
Q5 High-Fidelity DNA Polymerase	NEW ENGLAND BioLabs	Cat#: M0491S
Gibson Assembly Master Mix	NEW ENGLAND BioLabs	Cat#: E2611L
Quick Ligation Kit	NEW ENGLAND BioLabs	Cat#: M2200S
RQ1 RNase-free DNase	Promega	Cat#: M6101
qScript cDNA synthesis kit	Quanta Biosciences	Cat#: 95047-25
PerfeCTa SYBR Green FastMix	Quanta Biosciences	Cat#: 95073-250
Experimental Models: Organisms/Strains		
PY79 (*B. subtilis* wild type)	Youngman et al., 1984	NA
AR16 (*amyE*::P_{rrnE}-*gfp-spec*)	Rosenberg et al., 2012	NA
GD215 (Δ*hag*::*erm*)	Dubey and Ben-Yehuda, 2011	NA
GD110 (*amyE*::$P_{hyper\text{-}spank}$-*cat-spec*, pHB201/*cat*, *erm*)	Dubey and Ben-Yehuda, 2011	NA
GD267 (Δ*hag*::*erm*, *amyE*::$P_{hyper\text{-}spank}$-*cat-spec*)	Laboratory stock	NA
GD268 (Δ*hag*::*erm*, *amyE*::$P_{hyper\text{-}spank}$-*gfp-kan*)	Laboratory stock	NA
SB463 (*amyE*::$P_{hyper\text{-}spank}$-*cat-spec*)	Dubey and Ben-Yehuda, 2011	NA
SB513 (*amyE*::$P_{hyper\text{-}spank}$-*gfp-kan*)	Dubey and Ben-Yehuda, 2011	NA
GB61 (Δ*ymdB*::*tet*)	Dubey et al., 2016	NA
GB168 (Δ*ymdB*::*tet*, *amyE*::$P_{hyper\text{-}spank}$-*ymdB-spec*, Δ*hag*::*erm*)	Dubey et al., 2016	NA
IB11 (*Δmbl::erm*)	Bejerano-Sagie et al., 2006	NA
ET13 (*amyE*::$P_{hyper\text{-}spank}$-*yueB-yfp-spec*)	Tzipilevich et al., 2017	NA

(*Continued on next page*)

Continued

REAGENT or RESOURCE	SOURCE	IDENTIFIER
BDR524 (*amyE*::P_{xylA}-*spoIVFB-gfp-cat*)	Rudner et al., 2002	NA
SH8 (Δ*flgB-fliF::tet*, $P_{fla/che}$-*fliG-cheD*)	This study	NA
SH9 [Δ*CORE (fliO-flhA)::tet*, $P_{fla/che}$-*flhF-cheD*]	This study	NA
SH30 (Δ*fliO-flhA::tet*, $P_{fla/che}$-*flhF-cheD*, *amyE*::P_{rrnE}-*gfp-spec*)	This study	NA
SH31 (*sacA*::$P_{fla/che}$-*fliO-flhA-spec*)	This study	NA
SH33 (Δ*fliO-flhA::tet*, $P_{fla/che}$-*flhF-cheD*, *sacA*::$P_{fla/che}$-*fliO-flhA-spec*)	This study	NA
SH47 (*flhA-gfp-kan*)	This study	NA
SH55 (*flhA-gfp-kan*, Δ*ymdB::tet*, *amyE*::$P_{hyper\text{-}spank}$-*ymdB-spec*, Δ*hag::erm*)	This study	NA
SH79 (*sacA*::$P_{hyper\text{-}spank}$-*ymdB-kan*)	This study	NA
SH86 (*amyE*::$P_{hyper\text{-}spank}$-$fliP_{2xHA}$-*spec*)	This study	NA
SH93 (*amyE*::$P_{hyper\text{-}spank}$-$fliP_{2xHA}$-*spec*, *sacA*::$P_{hyper\text{-}spank}$-*ymdB-kan*)	This study	NA
SH103 (Δ*fliO::tet*, $P_{fla/che}$-*fliP-cheD*)	This study	NA
SH104 (Δ*fliP::tet*, $P_{fla/che}$-*fliQ-cheD*)	This study	NA
SH105 (Δ*fliQ::tet*, $P_{fla/che}$-*fliR-cheD*)	This study	NA
SH106 (Δ*fliR::tet*, $P_{fla/che}$-*flhB-cheD*)	This study	NA
SH107 (Δ*flhB::tet*, $P_{fla/che}$-*flhA-cheD*)	This study	NA
SH108 (Δ*flhA::tet*, $P_{fla/che}$-*flhF-cheD*)	This study	NA
SH110 (*amyE*::$P_{hyper\text{-}spank}$-$fliP_{2xHA}$-*spec*, *sacA*::$P_{hyper\text{-}spank}$-*ymdB-kan*, *Δmbl::erm*)	This study	NA
SH115 [*sacA*::$P_{fla/che}$-*CORE-*F_{Ec} (*fliOPQRflhBA*)-*spec*]	This study	NA
SH116 [Δ*fliO-flhA::tet*, *sacA*::$P_{fla/che}$-*CORE-*F_{Ec} (*fliOPQRflhBA*)-*spec*]	This study	NA
SH150 (*amyE*::$P_{hyper\text{-}spank}$-$fliP_{2xHA\text{-}LOOP}$-*spec*)	This study	NA
SH151 (*amyE*::$P_{hyper\text{-}spank}$-$fliP_{2xHA\text{-}LOOP}$-*spec*, *sacA*::$P_{hyper\text{-}spank}$-*ymdB-kan*)	This study	NA
SH161 (*amyE*::$P_{hyper\text{-}spank}$-$fliP_{2xHA\text{-}LOOP}$-*spec*, *sacA*::$P_{hyper\text{-}spank}$-*ymdB-kan*, *Δmbl::erm*)	This study	NA
SH169 [*amyE*::$P_{hyper\text{-}spank}$-*CORE-*F_{Ec} (*fliOPQRflhBA*)-*spec*]	This study	NA
SH170 [Δ*fliO-flhA::tet*, *amyE*::$P_{hyper\text{-}spank}$-*CORE-*F_{Ec} (*fliOPQRflhBA*)-*spec*]	This study	NA
SH177 (Δ*fliI::tet*, $P_{fla/che}$-*fliJ-cheD*)	This study	NA
SH203 (Δ*fliO::tet*, $P_{fla/che}$-*fliP-cheD*, *sacA*::$P_{fla/che}$-*fliO-spec*)	This study	NA
SH204 (Δ*fliP::tet*, $P_{fla/che}$-*fliQ-cheD*, *sacA*::$P_{fla/che}$-*fliP-spec*)	This study	NA
SH205 (Δ*fliQ::tet*, $P_{fla/che}$-*fliR-cheD*, *sacA*::$P_{fla/che}$-*fliQ-spec*)	This study	NA
SH206 (Δ*fliR::tet*, $P_{fla/che}$-*flhB-cheD*, *sacA*::$P_{fla/che}$-*fliR-spec*)	This study	NA
SH207 (Δ*flhB::tet*, $P_{fla/che}$-*flhA-cheD*, *sacA*::$P_{fla/che}$-*flhB-spec*)	This study	NA
SH208 (Δ*flhA::tet*, $P_{fla/che}$-*flhF-cheD*, *sacA*::$P_{fla/che}$-*flhA-spec*)	This study	NA
SH209 [Δ*fliO-flhA::tet*, *sacA*::$P_{fla/che}$-*CORE-*F_{Lm} (*fliPQRflhBA*)-*spec*]	This study	NA
SH210 [Δ*fliO-flhA::tet*, *sacA*::$P_{fla/che}$-*CORE-*F_{Bm} (*fliOPQRflhBA*)-*spec*]	This study	NA
SH244 (Δ*fliP::tet*, $P_{fla/che}$-*fliQ-cheD*, *sacA*::$P_{fla/che}$-*fliO-fliP-spec*)	This study	NA
SH245 (Δ*fliP::tet*, $P_{fla/che}$-*fliQ-cheD*, *sacA*::$P_{fla/che}$-*fliO-*$fliP_{2xHA}$-*spec*)	This study	NA
SH247 (Δ*fliP::tet*, $P_{fla/che}$-*fliQ-cheD*, *sacA*::$P_{fla/che}$-*fliO-*$fliP_{2xHA}$-*spec*, *Δmbl::erm*)	This study	NA
SH255 (*amyE*::$P_{hyper\text{-}spank}$-*yueB-yfp-spec*, *sacA*::$P_{hyper\text{-}spank}$-*ymdB-kan*)	This study	NA
SH256 (*amyE*::P_{xylA}-*spoIVFB-gfp-cat*, *sacA*::$P_{hyper\text{-}spank}$-*ymdB-kan*)	This study	NA
SH257 (*amyE*::$P_{hyper\text{-}spank}$-*yueB-yfp-spec*, *sacA*::$P_{hyper\text{-}spank}$-*ymdB-kan*, *Δmbl::erm*)	This study	NA
SH258 (*amyE*::P_{xylA}-*spoIVFB-gfp-cat*, *sacA*::$P_{hyper\text{-}spank}$-*ymdB-kan*, *Δmbl::erm*)	This study	NA
SH12 (Δ*flgB-fliF::tet*, $P_{fla/che}$-*fliG-cheD*, *amyE*::$P_{hyper\text{-}spank}$-*gfp-kan*)	This study	NA
SH13 (Δ*fliO-flhA::tet*, $P_{fla/che}$-*flhF-cheD*, *amyE*::$P_{hyper\text{-}spank}$-*gfp-kan*)	This study	NA
SH41 (Δ*fliO-flhA::tet*, $P_{fla/che}$-*flhF-cheD*, *sacA*::$P_{fla/che}$-*fliO-flhA-spec*, *amyE*::$P_{hyper\text{-}spank}$-*gfp-kan*)	This study	NA
SH119 (Δ*fliO::tet*, $P_{fla/che}$-*fliP-cheD*, *amyE*::$P_{hyper\text{-}spank}$-*gfp-kan*)	This study	NA

(*Continued on next page*)

Continued

REAGENT or RESOURCE	SOURCE	IDENTIFIER
SH120 (Δ*fliP::tet*, $P_{fla/che}$-*fliQ-cheD*, *amyE*::$P_{hyper\text{-}spank}$-*gfp-kan*)	This study	NA
SH121 (Δ*fliQ::tet*, $P_{fla/che}$-*fliR-cheD*, *amyE*::$P_{hyper\text{-}spank}$-*gfp-kan*)	This study	NA
SH122 (Δ*fliR::tet*, $P_{fla/che}$-*flhB-cheD*, *amyE*::$P_{hyper\text{-}spank}$-*gfp-kan*)	This study	NA
SH123 (Δ*flhB::tet*, $P_{fla/che}$-*flhA-cheD*, *amyE*::$P_{hyper\text{-}spank}$-*gfp-kan*)	This study	NA
SH124 (Δ*flhA::tet*, $P_{fla/che}$-*flhF-cheD*, *amyE*::$P_{hyper\text{-}spank}$-*gfp-kan*)	This study	NA
SH131 [Δ*fliO-flhA::tet*, *sacA*:: $P_{fla/che}$-*CORE-*F_{Ec} (*fliOPQRflhBA*)-*spec*, *amyE*::$P_{hyper\text{-}spank}$-*gfp-kan*]	This study	NA
SH182 (Δ*fliI::tet*, $P_{fla/che}$-*fliJ-cheD*, *amyE*::$P_{hyper\text{-}spank}$-*gfp-kan*)	This study	NA
SH213 (Δ*fliO::tet*, $P_{fla/che}$-*fliP-cheD, sacA*::$P_{fla/che}$-*fliO-spec*, *amyE*::$P_{hyper\text{-}spank}$-*gfp-kan*)	This study	NA
SH214 (Δ*fliP::tet*, $P_{fla/che}$-*fliQ-cheD, sacA*::$P_{fla/che}$-*fliP-spec*, *amyE*::$P_{hyper\text{-}spank}$-*gfp-kan*)	This study	NA
SH215 (Δ*fliQ::tet*, $P_{fla/che}$-*fliR-cheD, sacA*::$P_{fla/che}$-*fliQ-spec*, *amyE*::$P_{hyper\text{-}spank}$-*gfp-kan*)	This study	NA
SH216 (Δ*fliR::tet*, $P_{fla/che}$-*flhB-cheD, sacA*::$P_{fla/che}$-*fliR-spec*, *amyE*::$P_{hyper\text{-}spank}$-*gfp-kan*)	This study	NA
SH217 (Δ*flhB::tet*, $P_{fla/che}$-*flhA-cheD, sacA*::$P_{fla/che}$-*flhB-spec*, *amyE*::$P_{hyper\text{-}spank}$-*gfp-kan*)	This study	NA
SH218 (Δ*flhA::tet*, $P_{fla/che}$-*flhF-cheD, sacA*::$P_{fla/che}$-*flhA-spec*, *amyE*::$P_{hyper\text{-}spank}$-*gfp-kan*)	This study	NA
SH219 [Δ*fliO-flhA::tet*, *sacA*::$P_{fla/che}$-*CORE-*F_{Lm} (*fliPQRflhBA*)-*spec*, *amyE*::$P_{hyper\text{-}spank}$-*gfp-kan*]	This study	NA
SH220 [Δ*fliO-flhA::tet*, *sacA*::$P_{fla/che}$-*CORE-*F_{Bm} (*fliOPQRflhBA*)-*spec*, *amyE*::$P_{hyper\text{-}spank}$-*gfp-kan*]	This study	NA
SH248 (Δ*fliP::tet*, $P_{fla/che}$-*fliQ-cheD, sacA*::$P_{fla/che}$-*fliO-fliP-spec*, *amyE*::$P_{hyper\text{-}spank}$-*gfp-kan*)	This study	NA
SH16 (Δ*flgB-fliF::tet*, $P_{fla/che}$-*fliG-cheD*, *amyE*::$P_{hyper\text{-}spank}$ -*cat-spec*)	This study	NA
SH17 (Δ*fliO-flhA::tet*, $P_{fla/che}$-*flhF-cheD*, *amyE*::$P_{hyper\text{-}spank}$ -*cat-spec*)	This study	NA
SH58 (Δ*fliO-flhA::tet*, $P_{fla/che}$-*flhF-cheD*, *sacA*::$P_{fla/che}$-*fliO-flhA-spec*, *amyE*::$P_{hyper\text{-}spank}$-*cat-spec*)	This study	NA
SH125 (Δ*fliO::tet*, $P_{fla/che}$-*fliP-cheD*, *amyE*::$P_{hyper\text{-}spank}$-*cat-spec*)	This study	NA
SH126 (Δ*fliP::tet*, $P_{fla/che}$-*fliQ-cheD*, *amyE*::$P_{hyper\text{-}spank}$-*cat-spec*)	This study	NA
SH127 (Δ*fliQ::tet*, $P_{fla/che}$-*fliR-cheD*, *amyE*::$P_{hyper\text{-}spank}$-*cat-spec*)	This study	NA
SH128 (Δ*fliR::tet*, $P_{fla/che}$-*flhB-cheD*, *amyE*::$P_{hyper\text{-}spank}$-*cat-spec*)	This study	NA
SH129 (Δ*flhB::tet*, $P_{fla/che}$-*flhA-cheD*, *amyE*::$P_{hyper\text{-}spank}$-*cat-spec*)	This study	NA
SH130 (Δ*flhA::tet*, $P_{fla/che}$-*flhF-cheD*, *amyE*::$P_{hyper\text{-}spank}$-*cat-spec*)	This study	NA
SH132 [Δ*fliO-flhA::tet*, *sacA*:: $P_{fla/che}$-*CORE-*F_{Ec} (*fliOPQRflhBA*)-*spec*, *amyE*::$P_{hyper\text{-}spank}$-*cat-spec*]	This study	NA
SH183 (Δ*fliI::tet*, $P_{fla/che}$-*fliJ-cheD*, *amyE*::$P_{hyper\text{-}spank}$-*cat-spec*)	This study	NA
SH223 (Δ*fliO::tet*, $P_{fla/che}$-*fliP-cheD, sacA*::$P_{fla/che}$-*fliO-spec*, *amyE*::$P_{hyper\text{-}spank}$-*cat-spec*)	This study	NA
SH224 (Δ*fliP::tet*, $P_{fla/che}$-*fliQ-cheD, sacA*::$P_{fla/che}$-*fliP-spec*, *amyE*::$P_{hyper\text{-}spank}$-*cat-spec*)	This study	NA
SH225 (Δ*fliQ::tet*, $P_{fla/che}$-*fliR-cheD, sacA*::$P_{fla/che}$-*fliQ-spec*, *amyE*::$P_{hyper\text{-}spank}$-*cat-spec*)	This study	NA
SH226 (Δ*fliR::tet*, $P_{fla/che}$-*flhB-cheD, sacA*::$P_{fla/che}$-*fliR-spec*, *amyE*::$P_{hyper\text{-}spank}$-*cat-spec*)	This study	NA
SH227 (Δ*flhB::tet*, $P_{fla/che}$-*flhA-cheD, sacA*::$P_{fla/che}$-*flhB-spec*, *amyE*::$P_{hyper\text{-}spank}$-*cat-spec*)	This study	NA
SH228 (Δ*flhA::tet*, $P_{fla/che}$-*flhF-cheD, sacA*::$P_{fla/che}$-*flhA-spec*, *amyE*::$P_{hyper\text{-}spank}$-*cat-spec*)	This study	NA

(*Continued on next page*)

Continued

REAGENT or RESOURCE	SOURCE	IDENTIFIER
SH229 [Δ*fliO-flhA::tet*, *sacA*::$P_{fla/che}$-*CORE-F*$_{Lm}$ (*fliPQRflhBA*)-*spec*, *amyE*::$P_{hyper\text{-}spank}$-*cat-spec*]	This study	NA
SH230 [Δ*fliO-flhA::tet*, *sacA*::$P_{fla/che}$-*CORE-F*$_{Bm}$ (*fliOPQRflhBA*)-*spec*, *amyE*::$P_{hyper\text{-}spank}$-*cat-spec*]	This study	NA
SH249 (Δ*fliP::tet*, $P_{fla/che}$-*fliQ-cheD*, *sacA*::$P_{fla/che}$-*fliO-fliP-spec*, *amyE*::$P_{hyper\text{-}spank}$-*cat-spec*)	This study	NA
SH22 (Δ*flgB-fliF::tet*, $P_{fla/che}$-*fliG-cheD*, *amyE*::$P_{hyper\text{-}spank}$-*cat-spec*, pHB201/*cat*, *erm*)	This study	NA
SH23(Δ*fliO-flhA::tet*, $P_{fla/che}$-*flhF-cheD*, *amyE*::$P_{hyper\text{-}spank}$-*cat-spec*, pHB201/*cat*, *erm*)	This study	NA
SH62 (Δ*fliO-flhA::tet*, $P_{fla/che}$-*flhF-cheD*, *sacA*::$P_{fla/che}$-*fliO-flhA-spec*, *amyE*::$P_{hyper\text{-}spank}$-*cat-spec*, pHB201/*cat*, *erm*)	This study	NA
SH134 (Δ*fliO::tet*, $P_{fla/che}$-*fliP-cheD*, *amyE*::$P_{hyper\text{-}spank}$-*cat-spec*, pHB201/*cat*, *erm*)	This study	NA
SH135 (Δ*fliP::tet*, $P_{fla/che}$-*fliQ-cheD*, *amyE*::$P_{hyper\text{-}spank}$-*cat-spec*, pHB201/*cat*, *erm*)	This study	NA
SH136 (Δ*fliQ::tet*, $P_{fla/che}$-*fliR-cheD*, *amyE*::$P_{hyper\text{-}spank}$-*cat-spec*, pHB201/*cat*, *erm*)	This study	NA
SH137 (Δ*fliR::tet*, $P_{fla/che}$-*flhB-cheD*, *amyE*::$P_{hyper\text{-}spank}$-*cat-spec*, pHB201/*cat*, *erm*)	This study	NA
SH138 (Δ*flhB::tet*, $P_{fla/che}$-*flhA-cheD*, *amyE*::$P_{hyper\text{-}spank}$-*cat-spec*, pHB201/*cat*, *erm*)	This study	NA
SH139 (Δ*flhA::tet*, $P_{fla/che}$-*flhF-cheD*, *amyE*::$P_{hyper\text{-}spank}$-*cat-spec*, pHB201/*cat*, *erm*)	This study	NA
SH181 (Δ*hag*::*erm*, pHB201/*cat*, *erm*)	This study	NA
SH185 (Δ*fliI::tet*, $P_{fla/che}$-*fliJ-cheD*, *amyE*::$P_{hyper\text{-}spank}$-*cat-spec*, pHB201/*cat*, *erm*)	This study	NA
SH233 (Δ*fliO::tet*, $P_{fla/che}$-*fliP-cheD*, *sacA*::$P_{fla/che}$-*fliO-spec*, *amyE*::$P_{hyper\text{-}spank}$-*cat-spec*, pHB201/*cat*, *erm*)	This study	NA
SH234 (Δ*fliP::tet*, $P_{fla/che}$-*fliQ-cheD*, *sacA*::$P_{fla/che}$-*fliP-spec*, *amyE*::$P_{hyper\text{-}spank}$-*cat-spe*, pHB201/*cat*, *erm*)	This study	NA
SH235 (Δ*fliQ::tet*, $P_{fla/che}$-*fliR-cheD*, *sacA*::$P_{fla/che}$-*fliQ-spec*, *amyE*::$P_{hyper\text{-}spank}$-*cat-spe*, pHB201/*cat*, *erm*)	This study	NA
SH236 (Δ*fliR::tet*, $P_{fla/che}$-*flhB-cheD*, *sacA*::$P_{fla/che}$-*fliR-spec*, *amyE*::$P_{hyper\text{-}spank}$-*cat-spe*, pHB201/*cat*, *erm*)	This study	NA
SH237 (Δ*flhB::tet*, $P_{fla/che}$-*flhA-cheD*, *sacA*::$P_{fla/che}$-*flhB-spec*, *amyE*::$P_{hyper\text{-}spank}$-*cat-spec*, pHB201/*cat*, *erm*)	This study	NA
SH238 (Δ*flhA::tet*, $P_{fla/che}$-*flhF-cheD*, *sacA*::$P_{fla/che}$-*flhA-spec*, *amyE*::$P_{hyper\text{-}spank}$-*cat-spec*, pHB201/*cat*, *erm*)	This study	NA
SH239 [Δ*fliO-flhA::tet*, *sacA*::$P_{fla/che}$-*CORE-F*$_{Lm}$ (*fliPQRflhBA*)-*spec*, *amyE*::$P_{hyper\text{-}spank}$-*cat-spec*, pHB201/*cat*, *erm*]	This study	NA
SH240 [Δ*fliO-flhA::tet*, *sacA*::$P_{fla/che}$-*CORE-F*$_{Bm}$ (*fliOPQRflhBA*)-*spec*, *amyE*::$P_{hyper\text{-}spank}$-*cat-spec*, pHB201/*cat*, *erm*]	This study	NA
SH250 (Δ*fliP::tet*, $P_{fla/che}$-*fliQ-cheD*, *sacA*::$P_{fla/che}$-*fliO-fliP-spec*, *amyE*::$P_{hyper\text{-}spank}$-*cat-spec*, pHB201/*cat*, *erm*)	This study	NA
OS2 (*Bacillus megaterium* wild type isolate)	Stempler et al., 2017	NA
Bm Δ*CORE* (*fliO-flhA*)	This study	NA
Bm Δ*flagellin* (*hag*)	This study	NA
Escherichia coli K-12 MG1655	Laboratory stock	NA
XTL634 (Template for *tet*::*sacB* cassette)	Li et al., 2013	NA
RP7802 [*Escherichia coli* K-12 MG1655 Δ *fliOPQR*]	This study	NA
RP7809 [*Escherichia coli* K-12 MG1655 Δ*CORE* (*fliOPQRflhBA*)]	This study	NA

(*Continued on next page*)

Continued

REAGENT or RESOURCE	SOURCE	IDENTIFIER
Ec DY378 (1974) [W3110 λcI857, Δ(cro-*bioA*)]	Yu et al., 2000	
SK2462 (*Ec* DY378 Δ*fliC*::*kan*)	This study	NA
SK2468 [*Ec* K-12 MG1655 Δ*flagellin* (*fliC*::*kan*)]	This study	NA
Listeria monocytogenes 10403S	Kindly provided by Ran Nir-Paz (Hebrew U)	NA
Lm 10403S Δ*CORE* (*fliP-flhA*)	This study	NA
Lm 10403S Δ *flagellin* (*flaA*)	This study	NA
Oligonucleotides		
Primers used in this study are listed in Table S3.	All primers were designed during this study, and synthesized by Integrated DNA Technologies (IDT).	NA
Recombinant DNA		
pDR111 (*amyE*::$P_{hyper\text{-}spank}$-*spec*)	Kindly provided by David Rudner (Harvard U)	NA
pHB201 (*cat*, *erm*)	Bron et al., 1998	NA
pKL168 (*gfp-kan*)	Lemon and Grossman, 1998	NA
pKD46 (λ RED genes, Amp^r)	Datsenko and Wanner, 2000	NA
pRP7358 [P_{tac}-*CORE*-F_{Ec} (*fliOPQRflhBA*)]	Pal et al., 2019	NA
pSH13 (*flhA-gfp-kan*)	This study	NA
pSH17 (*amyE*::$P_{hyper\text{-}spank}$-$fliP_{2xHA}$-*spec*)	This study	NA
pSH19 (*amyE*::$P_{hyper\text{-}spank}$-$fliP_{2xHA\text{-}LOOP}$-*spec*)	This study	NA
pSH21 [*amyE*::$P_{hyper\text{-}spank}$- *CORE*-F_{Ec} (*fliOPQRflhBA*)-*spec*]	This study	NA
pLR16- Phes	Kindly provided by Anat Herskovits (Tel Aviv U) (Argov et al., 2017)	NA
pLR16-AB1	This study	NA
pSH22 (pLR16-*Lm flaA* int)	This study	NA
pSH23 (pDG1514-*Bm hag* int)	This study	NA
Other		
Carbon film on 300 square mesh copper grids	Electron Microscopy Sciences	Cat#: CF300-Cu
Lysing Matrix B Bulk	MP Biomedicals	Cat#: 6540-428

CONTACT FOR REAGENT AND RESOURCE SHARING

Further information and requests for resources and reagents should be directed to and will be fulfilled by the Lead Contact, Sigal Ben-Yehuda (sigalb@ekmd.huji.ac.il).

EXPERIMENTAL MODEL AND SUBJECT DETAILS

Details on bacterial strain construction

Bs strains are derivatives of the wild-type strain PY79, *Bm* is a wild-type soil isolate (OS2), *Ec* strains are derivatives of the wild-type strain K-12 MG1655, *Lm* strains are derivatives of the wild-type strain 10403S. Bacterial strains and plasmids are listed in Key resources table, and primers are listed in Table S3.

For gene replacement strategy in *Bs*, indicated primer pairs (P1-P4; Table S3) were used to amplify the flanking genomic regions of the corresponding gene. The *fla/che* promoter region was amplified using the primers P_{flgB}1-2. PCR products were used for Gibson assembly (NEB, USA), together with the respective antibiotic resistance gene (Guérout-Fleury et al., 1996) The resultant product was used to transform PY79 to obtain the mutant allele.

SH8 (Δ*flgB-fliF::tet,* $P_{fla/che}$-*fliG-cheD*) was constructed using Gibson assembly kit (NEB, USA) utilizing primers *flgB-fliF* KO P1-P4 and P_{flgB}1-2. **SH9** (Δ*fliO-flhA::tet,* $P_{fla/che}$-*flhF-cheD*) was constructed using Gibson assembly kit (NEB, USA) utilizing primers *CORE* KO P1-P4 and P_{flgB}1-2. **SH12** (Δ*flgB-fliF::tet,* $P_{fla/che}$-*fliG-cheD*, *amyE*::$P_{hyper\text{-}spank}$-*gfp-kan*) was constructed by transforming SH8 with genomic DNA (gDNA) from strain SB513. **SH13** (Δ*fliO-flhA::tet,* $P_{fla/che}$-*flhF-cheD*, *amyE*::$P_{hyper\text{-}spank}$-*gfp-kan*) was constructed by transforming SH9 with gDNA from strain SB513. **SH16** (Δ*flgB-fliF::tet,* $P_{fla/che}$-*fliG-cheD*, *amyE*:: $P_{hyper\text{-}spank}$-*cat-spec*) was constructed by transforming SH8 with gDNA from strain SB463. **SH17** (Δ*fliO-flhA::tet,* $P_{fla/che}$-*flhF-cheD*, *amyE*:: $P_{hyper\text{-}spank}$ -*cat-spec*) was

constructed by transforming SH9 with gDNA from strain SB463. **SH22** (Δ*flgB-fliF::tet,* $P_{fla/che}$-*fliG-cheD*, *amyE*::$P_{hyper\text{-}spank}$-*cat-spec*, pHB201/*cat*, *erm*) was constructed by transforming SH8 with pHB201. **SH23** (Δ*fliO-flhA::tet,* $P_{fla/che}$-*flhF-cheD*, *amyE*::$P_{hyper\text{-}spank}$-*cat-spec*, pHB201/*cat*, *erm*) was constructed by transforming SH9 with pHB201. **SH30** (Δ*fliO-flhA::tet,*$P_{fla/che}$-*flhF-cheD*, *amyE::*P_{rrnE}-*gfp-spec*) was constructed by transforming gDNA SH9 with from strain AR16. **SH31** (*sacA::*$P_{fla/che}$-*fliO-flhA-spec*) was constructed using Gibson assembly kit (NEB, USA) utilizing primers *sacA* P1-P4, *Bs CORE* comp1-2 and Comp P_{flgB}1-2. **SH33** (Δ*fliO-flhA::tet,* $P_{fla/che}$-*flhF-cheD*, *sacA::*$P_{fla/che}$-*fliO-flhA-spec*) was constructed by transforming SH9 with gDNA from strain SH31. **SH41** (Δ*fliO-flhA::tet,* $P_{fla/che}$-*flhF-cheD*, *sacA::*$P_{fla/che}$-*fliO-flhA-spec, amyE*::$P_{hyper\text{-}spank}$-*gfp-kan*) was constructed by transforming SH33 with gDNA from strain SB513. **SH47** (*flhA-gfp-kan)* was constructed by transforming PY79 with pSH13. **SH55** (*flhA-gfp-kan*, Δ*ymdB*::*tet*, *amyE*::$P_{hyper\text{-}spank}$-*ymdB-spec*, Δ*hag*::*erm)* was constructed by transforming GB168 with gDNA from strain SH47. **SH58** (Δ*fliO-flhA::tet,* $P_{fla/che}$-*flhF-cheD*, *sacA::*$P_{fla/che}$-*fliO-flhA-spec*, *amyE*::$P_{hyper\text{-}spank}$-*cat-spec*) was constructed by transforming SH33 with gDNA from strain SB463. **SH62** (Δ*fliO-flhA::tet,* $P_{fla/che}$-*flhF-cheD*, *sacA::*$P_{fla/che}$-*fliO-flhA-spec*, *amyE*::$P_{hyper\text{-}spank}$-*cat-spec*, pHB201/*cat*, *erm*) was constructed by transforming SH58 with pHB201. **SH79** (*sacA*::$P_{hyper\text{-}spank}$-*ymdB-kan*) was constructed using Gibson assembly kit (NEB, USA) utilizing primers *sacA* P1-P4 and Comp P_{HS}1-*ymdB* R. $P_{hyper\text{-}spank}$-*ymdB* was amplified from GB168 gDNA using Comp P_{HS}1-*ymdB* R primers. **SH86** (*amyE*::$P_{hyper\text{-}spank}$-$fliP_{2xHA}$-*spec*) was constructed by transforming PY79 with pSH17. **SH93** (*amyE*::$P_{hyper\text{-}spank}$-$fliP_{2xHA}$-*spec*, *sacA*::$P_{hyper\text{-}spank}$-*ymdB-kan*) was constructed by transforming SH79 with gDNA from strain SH86. **SH96** (*flhA-gfp-kan*, *amyE::*P_{hag}-hag^{T209C}-*spec*) was constructed by transforming DS1895 with gDNA from strain SH47. **SH103** (Δ*fliO::tet,* $P_{fla/che}$-*fliP-cheD*) was constructed using Gibson assembly kit (NEB, USA) utilizing primers *fliO* KO P1-P4 and P_{flgB}1-2. **SH104** (Δ*fliP::tet,* $P_{fla/che}$-*fliQ-cheD*) was constructed using Gibson assembly kit (NEB, USA) utilizing primers *fliP* KO P1-P4 and P_{flgB}1-2. **SH105** (Δ*fliQ::tet,* $P_{fla/che}$-*fliR-cheD*) was constructed using Gibson assembly kit (NEB, USA) utilizing primers *fliQ* KO P1-P4 and P_{flgB}1-2. **SH106** (Δ*fliR::tet,* $P_{fla/che}$-*flhB-cheD*) was constructed using Gibson assembly kit (NEB, USA) utilizing primers *fliR* KO P1-P4 and P_{flgB}1-2. **SH107** (Δ*flhB::tet,* $P_{fla/che}$-*flhA-cheD*) was constructed using Gibson assembly kit (NEB, USA) utilizing primers *flhB* KO P1-P4 and P_{flgB}1-2. **SH108** (Δ*flhA::tet,* $P_{fla/che}$-*flhF-cheD*) was constructed using Gibson assembly kit (NEB, USA) utilizing primers *flhA* KO P1-P4 and P_{flgB}1-2. **SH110** (*amyE*::$P_{hyper\text{-}spank}$-$fliP_{2xHA}$-*spec*, *sacA*::$P_{hyper\text{-}spank}$-*ymdB-kan, Δmbl::erm*) was constructed by transforming SH93 with gDNA from strain IB11. **SH115** [*sacA::*$P_{fla/che}$-*CORE-*F_{Ec} (*fliOPQRflhBA*)-*spec*] was constructed using Gibson assembly kit (NEB, USA) utilizing primers *sacA* P1-P4, *Ec CORE* comp 1-2 and Comp P_{flgB}1-2a. *CORE-*F_{Ec} (*fliOPQRflhBA*) was amplified from pRP7358 using primers *Ec CORE* comp 1-2. **SH116** [Δ*fliO-flhA::tet*, *sacA:* $P_{fla/che}$-*CORE-*F_{Ec} (*fliOPQRflhBA*)-*spec*] was constructed by transforming SH9 with gDNA from strain SH115. **SH119** (Δ*fliO::tet,* $P_{fla/che}$-*fliP-cheD*, *amyE*::$P_{hyper\text{-}spank}$-*gfp-kan*) was constructed by transforming SH103 with gDNA from strain SB513. **SH120** (Δ*fliP::tet,* $P_{fla/che}$-*fliQ-cheD*, *amyE*::$P_{hyper\text{-}spank}$-*gfp-kan*) was constructed by transforming SH104 with gDNA from strain SB513. **SH121** (Δ*fliQ::tet,* $P_{fla/che}$-*fliR-cheD*, *amyE*::$P_{hyper\text{-}spank}$-*gfp-kan*) was constructed by transforming SH105 with gDNA from strain SB513. **SH122** (Δ*fliR::tet,* $P_{fla/che}$-*flhB-cheD*, *amyE*::$P_{hyper\text{-}spank}$-*gfp-kan*)was constructed by transforming SH106 with gDNA from strain SB513. **SH123** (Δ*flhB::tet,* $P_{fla/che}$-*flhA-cheD*, *amyE*::$P_{hyper\text{-}spank}$-*gfp-kan*) was constructed by transforming SH107 with gDNA from strain SB513. **SH124** (Δ*flhA::tet,* $P_{fla/che}$-*flhF-cheD*, *amyE*::$P_{hyper\text{-}spank}$-*gfp-kan*) was constructed by transforming SH108 with gDNA from strain SB513. **SH125** (Δ*fliO::tet,* $P_{fla/che}$-*fliP-cheD*, *amyE*::$P_{hyper\text{-}spank}$-*cat-spec*) was constructed by transforming SH103 with gDNA from strain SB463. **SH126** (Δ*fliP::tet,* $P_{fla/che}$-*fliQ-cheD*, *amyE*::$P_{hyper\text{-}spank}$-*cat-spec*) was constructed by transforming SH104 with gDNA from strain SB463. **SH127** (Δ*fliQ::tet,* $P_{fla/che}$-*fliR-cheD*, *amyE*::$P_{hyper\text{-}spank}$-*cat-spec*) was constructed by transforming SH105 with gDNA from strain SB463. **SH128** (Δ*fliR::tet,* $P_{fla/che}$-*flhB-cheD*, *amyE*::$P_{hyper\text{-}spank}$-*cat-spec*) was constructed by transforming SH106 with gDNA from strain SB463. **SH129** (Δ*flhB::tet,* $P_{fla/che}$-*flhA-cheD*, *amyE*::$P_{hyper\text{-}spank}$-*cat-spec*) was constructed by transforming SH107 with gDNA from strain SB463. **SH130** (Δ*flhA::tet,* $P_{fla/che}$-*flhF-cheD*, *amyE*::$P_{hyper\text{-}spank}$-*cat-spec*) was constructed by transforming SH108 with gDNA from strain SB463. **SH131** [Δ*fliO-flhA::tet*, *sacA::* $P_{fla/che}$-*CORE-*F_{Ec} (*fliOPQRflhBA*)-*spec*, *amyE*::$P_{hyper\text{-}spank}$-*gfp-kan*] was constructed by transforming SH116 with gDNA from strain SB513. **SH132** [Δ*fliO-flhA::tet*, *sacA::*$P_{fla/che}$-*CORE-*F_{Ec} (*fliOPQRflhBA*)-*spec*, *amyE*::$P_{hyper\text{-}spank}$-*cat-spec*] was constructed by transforming SH116 with gDNA from strain SB463. **SH134** (Δ*fliO::tet,* $P_{fla/che}$-*fliP-cheD*, *amyE*::$P_{hyper\text{-}spank}$-*cat-spec*) was constructed by transforming SH125 with pHB201. **SH135** (Δ*fliP::tet,* $P_{fla/che}$-*fliQ-cheD*, *amyE*::$P_{hyper\text{-}spank}$-*cat-spec*) was constructed by transforming SH126 with pHB201. **SH136** (Δ*fliQ::tet,* $P_{fla/che}$-*fliR-cheD*, *amyE*::$P_{hyper\text{-}spank}$-*cat-spec*) was constructed by transforming SH127 with pHB201. **SH137** (Δ*fliR::tet,* $P_{fla/che}$-*flhB-cheD*, *amyE*::$P_{hyper\text{-}spank}$-*cat-spec*) was constructed by transforming SH128 with pHB201. **SH138** (Δ*flhB::tet,* $P_{fla/che}$-*flhA-cheD*, *amyE*::$P_{hyper\text{-}spank}$-*cat-spec*) was constructed by transforming SH129 with pHB201. **SH139** (Δ*flhA::tet,* $P_{fla/che}$-*flhF-cheD*, *amyE*::$P_{hyper\text{-}spank}$-*cat-spec*) was constructed by transforming SH130 with pHB201. **SH150** (*amyE*::$P_{hyper\text{-}spank}$-$fliP_{2xHA\text{-}LOOP}$-*spec*) was constructed by transforming PY79 with pSH19. **SH151** (*amyE*::$P_{hyper\text{-}spank}$-$fliP_{2xHA\text{-}LOOP}$-*spec*, *sacA*::$P_{hyper\text{-}spank}$-*ymdB-kan*) was constructed by transforming SH79 with gDNA from strain SH150. **SH161** (*amyE*::$P_{hyper\text{-}spank}$-$fliP_{2xHA\text{-}LOOP}$-*spec*, *sacA*::$P_{hyper\text{-}spank}$-*ymdB-kan*, *Δmbl::erm*) was constructed by transforming SH150 with gDNA from strain IB11. **SH169** [*amyE::*$P_{hyper\text{-}spank}$-*CORE-*F_{Ec} (*fliOPQRflhBA*)-*spec*] was constructed by transforming PY79 with pSH21. **SH170** [Δ*fliO-flhA::tet*, *amyE::*$P_{hyper\text{-}spank}$-*CORE-*F_{Ec} (*fliOPQRflhBA*)-*spec*] was constructed by transforming SH9 with gDNA from strain SH169. **SH177** (Δ*fliI::tet,* $P_{fla/che}$-*fliJ-cheD*) was constructed using Gibson assembly kit (NEB, USA) utilizing primers *fli*I KO P1-P4 and P_{flgB}1-2. **SH181** (Δ*hag*::*erm*, pHB201/*cat*, *erm*) was constructed by transforming GD215 with pHB201. **SH182** (Δ*fliI::tet,* $P_{fla/che}$-*fliJ-cheD*, *amyE*::$P_{hyper\text{-}spank}$-*gfp-kan*) was constructed by transforming SH177 with gDNA from strain SB513. **SH183** (Δ*fliI::tet,* $P_{fla/che}$-*fliJ-cheD*, *amyE*::$P_{hyper\text{-}spank}$-*cat-spec*) was constructed by transforming SH177 with gDNA from strain SB463. **SH185** (Δ*fliI::tet,* $P_{fla/che}$-*fliJ-cheD*, *amyE*::$P_{hyper\text{-}spank}$-*cat-spec*, pHB201/*cat*, *erm*) was constructed by transforming SH183 with pHB201. **SH203** (Δ*fliO::tet,* $P_{fla/che}$-*fliP-cheD, sacA::*$P_{fla/che}$-*fliO-spec*) was constructed by transforming SH103 with complementation

construct generated using Gibson assembly kit (NEB, USA) utilizing primers *sacA* P1-P4, *fliO* comp1-2 and Comp P_{flgB}1-R. **SH204** (Δ*fliP::tet,* $P_{fla/che}$-*fliQ-cheD, sacA::*$P_{fla/che}$-*fliP-spec*) was constructed by transforming SH104 with complementation construct generated using Gibson assembly kit (NEB, USA) utilizing primers *sacA* P1-P4, *fliP* comp1-2 and Comp P_{flgB}1-R. **SH205** (Δ*fliQ::tet,* $P_{fla/che}$-*fliR-cheD, sacA::*$P_{fla/che}$-*fliQ-spec*) was constructed by transforming SH105 with complementation construct generated using Gibson assembly kit (NEB, USA) utilizing primers *sacA* P1-P4, *fliQ* comp1-2 and Comp P_{flgB}1-R. **SH206** (Δ*fliR::tet,* $P_{fla/che}$-*flhB-cheD, sacA::* $P_{fla/che}$-*fliR-spec*) was constructed by transforming SH106 with complementation construct generated using Gibson assembly kit (NEB, USA) utilizing primers *sacA* P1-P4, *fliR* comp1-2 and Comp P_{flgB}1-R. **SH207** (Δ*flhB::tet,* $P_{fla/che}$-*flhA-cheD, sacA::*$P_{fla/che}$-*flhB-spec*) was constructed by transforming SH107 with complementation construct generated using Gibson assembly kit (NEB, USA) utilizing primers *sacA* P1-P4, *flhB* comp1-2 and Comp P_{flgB}1-R. **SH208** (Δ*flhA::tet,* $P_{fla/che}$-*flhF-cheD, sacA::*$P_{fla/che}$-*flhA-spec*) was constructed by transforming SH108 with complementation construct generated using Gibson assembly kit (NEB, USA) utilizing primers *sacA* P1-P4, *flhA* comp1-2 and Comp P_{flgB}1-R. **SH209** [Δ*fliO-flhA::tet*, *sacA::*$P_{fla/che}$-*CORE-*F_{Lm} (*fliPQRflhBA*)-*spec*] was constructed by transforming SH9 with complementation construct generated using Gibson assembly kit (NEB, USA) utilizing primers *sacA* P1-P4, *Lm CORE* comp1-2 and Comp P_{flgB}1-R. *CORE-*F_{Lm} (*fliPQRflhBA*) was amplified from *Lm* (10403S) gDNA using primers *Lm CORE* comp 1-2. **SH210** [Δ*fliO-flhA::tet*, *sacA::*$P_{fla/che}$-*CORE-*F_{Bm} (*fliOPQRflhBA*)-*spec*] was constructed by transforming SH9 with complementation construct generated using Gibson assembly kit (NEB, USA) utilizing primers *sacA* P1-P4, *Bm CORE* comp1-2 and Comp P_{flgB}1-R. *CORE-*F_{Bm} (*fliOPQRflhBA*) was amplified from *Bm* (OS2) gDNA using primers *Bm CORE* comp 1-2. **SH213** (Δ*fliO::tet,* $P_{fla/che}$-*fliP-cheD, sacA::*$P_{fla/che}$-*fliO-spec*, *amyE*::$P_{hyper\text{-}spank}$-*gfp-kan*) was constructed by transforming SH203 with gDNA from strain SB513. **SH214** (Δ*fliP::tet,* $P_{fla/che}$-*fliQ-cheD, sacA::*$P_{fla/che}$-*fliP-spec*, *amyE*::$P_{hyper\text{-}spank}$-*gfp-kan*) was constructed by transforming SH204 with gDNA from strain SB513. **SH215** (Δ*fliQ::tet,* $P_{fla/che}$-*fliR-cheD, sacA::*$P_{fla/che}$-*fliQ-spec*, *amyE*::$P_{hyper\text{-}spank}$-*gfp-kan*) was constructed by transforming SH205 with gDNA from strain SB513. **SH216** (Δ*fliR::tet,* $P_{fla/che}$-*flhB-cheD, sacA::*$P_{fla/che}$-*fliR-spec*, *amyE*::$P_{hyper\text{-}spank}$-*gfp-kan*) was constructed by transforming SH206 with gDNA from strain SB513. **SH217** (Δ*flhB::tet,* $P_{fla/che}$-*flhA-cheD, sacA::*$P_{fla/che}$-*flhB-spec*, *amyE*::$P_{hyper\text{-}spank}$-*gfp-kan*) was constructed by transforming SH207 with gDNA from strain SB513. **SH218** (Δ*flhA::tet,* $P_{fla/che}$-*flhF-cheD, sacA::*$P_{fla/che}$-*flhA-spec*, *amyE*::$P_{hyper\text{-}spank}$-*gfp-kan*) was constructed by transforming SH208 with gDNA from strain SB513. **SH219** [Δ*fliO-flhA::tet*, *sacA::*$P_{fla/che}$-*CORE-*F_{Lm} (*fliPQRflhBA*)-*spec*, *amyE*::$P_{hyper\text{-}spank}$-*gfp-kan*] was constructed by transforming SH209 with gDNA from strain SB513. **SH220** [Δ*fliO-flhA::tet*, *sacA::*$P_{fla/che}$-*CORE-*F_{Bm} (*fliOPQRflhBA*)-*spec*, *amyE*::$P_{hyper\text{-}spank}$-*gfp-kan*] was constructed by transforming SH210 with gDNA from strain SB513. **SH223** (Δ*fliO::tet,* $P_{fla/che}$-*fliP-cheD, sacA::*$P_{fla/che}$-*fliO-spec*, *amyE*::$P_{hyper\text{-}spank}$-*cat-spec*) was constructed by transforming SH203 with gDNA from strain SB463. **SH224** (Δ*fliP::tet,* $P_{fla/che}$-*fliQ-cheD, sacA::*$P_{fla/che}$-*fliP-spec*, *amyE*::$P_{hyper\text{-}spank}$-*cat-spec*) was constructed by transforming SH204 with gDNA from strain SB463. **SH225** (Δ*fliQ::tet,* $P_{fla/che}$-*fliR-cheD, sacA::*$P_{fla/che}$-*fliQ-spec*, *amyE*::$P_{hyper\text{-}spank}$-*cat-spec*) was constructed by transforming SH205 with gDNA from strain SB463. **SH226** (Δ*fliR::tet,* $P_{fla/che}$-*flhB-cheD, sacA::*$P_{fla/che}$-*fliR-spec*, *amyE*::$P_{hyper\text{-}spank}$-*cat-spec*) was constructed by transforming SH206 with gDNA from strain SB463. **SH227** (Δ*flhB::tet,* $P_{fla/che}$-*flhA-cheD, sacA::*$P_{fla/che}$-*flhB-spec*, *amyE*::$P_{hyper\text{-}spank}$-*cat-spec*) was constructed by transforming SH207 with gDNA from strain SB463. **SH228** (Δ*flhA::tet,* $P_{fla/che}$-*flhF-cheD, sacA::*$P_{fla/che}$-*flhA-spec*, *amyE*::$P_{hyper\text{-}spank}$-*cat-spec*) was constructed by transforming SH208 with gDNA from strain SB463. **SH229** [Δ*fliO-flhA::tet*, *sacA::*$P_{fla/che}$-*CORE-*F_{Lm}(*fliPQRflhBA*)-*spec*, *amyE*::$P_{hyper\text{-}spank}$-*cat-spec*] was constructed by transforming SH209 with gDNA from strain SB463. **SH230** [Δ*fliO-flhA::tet*, *sacA::*$P_{fla/che}$-*CORE-*F_{Bm} (*fliOPQRflhBA*)-*spec*, *amyE*::$P_{hyper\text{-}spank}$-*cat-spec*] was constructed by transforming SH210 with gDNA from strain SB463. **SH233** (Δ*fliO::tet,* $P_{fla/che}$-*fliP-cheD, sacA::*$P_{fla/che}$-*fliO-spec*, *amyE*::$P_{hyper\text{-}spank}$-*cat-spec*, pHB201/*cat*, *erm*) was constructed by transforming SH223 with pHB201. **SH234** (Δ*fliP::tet,* $P_{fla/che}$-*fliQ-cheD, sacA::*$P_{fla/che}$-*fliP-spec*, *amyE*::$P_{hyper\text{-}spank}$-*cat-spe*, pHB201/*cat*, *erm*) was constructed by transforming SH224 with pHB201. **SH235** (Δ*fliQ::tet,* $P_{fla/che}$-*fliR-cheD, sacA::*$P_{fla/che}$-*fliQ-spec*, *amyE*::$P_{hyper\text{-}spank}$-*cat-spe*, pHB201/*cat*, *erm*) was constructed by transforming SH225 with pHB201. **SH236** (Δ*fliR::tet,* $P_{fla/che}$-*flhB-cheD, sacA::*$P_{fla/che}$-*fliR-spec*, *amyE*::$P_{hyper\text{-}spank}$-*cat-spe*, pHB201/*cat*, *erm*) was constructed by transforming SH226 with pHB201. **SH237** (Δ*flhB::tet,* $P_{fla/che}$-*flhA-cheD, sacA::*$P_{fla/che}$-*flhB-spec*, *amyE*::$P_{hyper\text{-}spank}$-*cat-spec*, pHB201/*cat*, *erm*) was constructed by transforming SH227 with pHB201. **SH238** (Δ*flhA::tet,* $P_{fla/che}$-*flhF-cheD, sacA::*$P_{fla/che}$-*flhA-spec*, *amyE*::$P_{hyper\text{-}spank}$-*cat-spec*, pHB201/*cat*, *erm*) was constructed by transforming SH228 with pHB201. **SH239** [Δ*fliO-flhA::tet*, *sacA::*$P_{fla/che}$-*CORE-*F_{Lm} (*fliPQRflhBA*)-*spec*, *amyE*::$P_{hyper\text{-}spank}$-*cat-spec*, pHB201/*cat*, *erm*] was constructed by transforming SH229 with pHB201. **SH240** [Δ*fliO-flhA::tet*, *sacA::*$P_{fla/che}$-*CORE-*F_{Bm} (*fliOPQRflhBA*)-*spec*, *amyE*::$P_{hyper\text{-}spank}$-*cat-spec*, pHB201/*cat*, *erm*] was constructed by transforming SH230 with pHB201. **SH244** (Δ*fliP::tet,* $P_{fla/che}$-*fliQ-cheD, sacA::*$P_{fla/che}$-*fliO-fliP-spec*) was constructed by transforming SH104 with complementation construct generated using Gibson assembly kit (NEB, USA) utilizing primers *sacA* P1-P4, *fliO* comp 1-*fliP* comp 2 and Comp P_{flgB}1-R. **SH245** (Δ*fliP::tet,* $P_{fla/che}$-*fliQ-cheD, sacA::*$P_{fla/che}$-*fliO-fliP*$_{2xHA}$-*spec*) was constructed by transforming SH104 with complementation construct generated using Gibson assembly kit (NEB, USA) utilizing primers *sacA* P1-P4, Comp P_{flgB}1-R, and $fliOP_{2xHA}$ construct. *fliOP* was amplified using *fliO* comp 1 and *fliP* ORF R (2X HA), followed by a second round of PCR using primers *fliP* comp 1 and 2X HA R to finally obtain $fliOP_{2xHA}$ construct. **SH247** (Δ*fliP::tet,* $P_{fla/che}$-*fliQ-cheD, sacA::*$P_{fla/che}$-*fliO-fliP*$_{2xHA}$-*spec, Δmbl::erm*) was constructed by transforming SH245 with gDNA from strain IB11. **SH248** (Δ*fliP::tet,* $P_{fla/che}$-*fliQ-cheD, sacA::*$P_{fla/che}$-*fliO-fliP-spec*, *amyE*::$P_{hyper\text{-}spank}$-*gfp-kan*) was constructed by transforming SH244 with gDNA from strain SB513. **SH249** (Δ*fliP::tet,* $P_{fla/che}$-*fliQ-cheD, sacA::*$P_{fla/che}$-*fliO-fliP-spec*, *amyE*::$P_{hyper\text{-}spank}$-*cat-spec*) was constructed by transforming SH244 with gDNA from strain SB463. **SH250** (Δ*fliP::tet,* $P_{fla/che}$-*fliQ-cheD, sacA::*$P_{fla/che}$-*fliO-fliP-spec*, *amyE*::$P_{hyper\text{-}spank}$-*cat-spec*, pHB201/*cat*, *erm*) was constructed by transforming SH249 with pHB201. **SH255** (*amyE*::$P_{hyper\text{-}spank}$-*yueB-yfp-spec, sacA*::$P_{hyper\text{-}spank}$-*ymdB-kan*) was constructed by transforming ET13 with gDNA from strain SH79. **SH256** (*amyE*::P_{xylA}-*spoIVFB-gfp-cat, sacA*::$P_{hyper\text{-}spank}$-*ymdB-kan*) was constructed by transforming BDR524 with gDNA from

strain SH79. **SH257** (*amyE*::$P_{hyper\text{-}spank}$-*yueB-yfp-spec, sacA*::$P_{hyper\text{-}spank}$-*ymdB-kan, Δmbl::erm*) was constructed by transforming ET13 with gDNA from strain IB11. **SH258** (*amyE*::P_{xylA}-*spoIVFB-gfp-cat, sacA*::$P_{hyper\text{-}spank}$-*ymdB-kan, Δmbl::erm*) was constructed by transforming BDR524 with gDNA from strain IB11.

METHOD DETAILS

General growth conditions

All general methods for *Bs* were carried out as described previously (Harwood and Cutting, 1990). *Bs* cultures were inoculated at OD_{600} 0.05 from an overnight culture and growth was carried out at 37°C in LB medium (Difco). For strains harboring genes under inducible promoters, 1 mM IPTG (Sigma-Aldrich) or 0.5% xylose (Sigma-Aldrich) was added to the medium. Antibiotics were used at the following concentrations: kanamycin (5 μg/ml, US Biological), chloramphenicol (6 μg/ml, Sigma-Aldrich), lincomycin (25 μg/ml, Sigma-Aldrich), erythromycin (1 μg/ml, Sigma-Aldrich), tetracycline (10 μg/ml, Sigma-Aldrich), spectinomycin (100 μg/ml, Sigma-Aldrich).

Transformation into *Bm* (OS2) cells was carried out as previously described (Moro et al., 1995). *Bm* cells were grown up to 1.0 OD_{600} (10 ml). Cells were then washed with electroporation buffer [25% PEG 8000 (Promega) and 0.1 M sorbitol (Sigma-Aldrich)] and resuspended in 1 mL of the same buffer. Electroporation was carried out with 0.1 mL of cells supplemented with 500 ng of linear DNA or plasmid DNA at 1500 V (Bio-Rad). Cells were then resuspended in 1 mL LB, incubated at 37°C for 1 hr, and plated on LB plates containing 5 μg/ml tetracycline.

Scarless deletions of *E. coli* were constructed using λ Red system and *tet-sacB* cassette as described (Datsenko and Wanner, 2000; Li et al., 2013). 50 bp of upstream and downstream sequences of *fliOPQR* ORFs were included in the forward primer 3907 and reverse primer 3908, respectively. These primers were used for PCR amplifying *tet-sacB* cassette from XTL634. Next, the cassette was inserted into MG1655 strain, containing pKD46 carrying λ Red genes (γ, β and *exo*) and a temperature sensitive origin. Around 1 Kb of recombination sequences upstream and downstream of *fliOPQR* were PCR amplified using primers 3909, 3912, 3950 and 3951. The upstream and downstream recombination sequences were ligated together by isothermal assembly (Gibson, 2011). The *tet-sacB* cassette was then replaced with the ligated DNA using similar λ Red system and selected on 6% sucrose (J.T.Baker). Next, the plasmid pKD46 was cured at 42°C to construct the strain **RP7802** (Δ*fliOPQR*). Next, *tet-sacB* cassette was PCR amplified using primers 3914 and 3915. The cassette was inserted in RP7802 strain containing pKD46 using λ Red system. Around 1 Kb of recombination sequences upstream and downstream of *flhBA* were PCR amplified using primers 3952, 3953, 3954 and 3955. The upstream and downstream recombination sequences were ligated together by isothermal assembly and the *tet-sacB* cassette was then replaced with the ligated DNA using similar λ Red system. Next, the plasmid pKD46 was cured, and strain **RP7809** (Δ*CORE* [*fliOPQRflhBA*]) constructed. Δ*fliC*::*kan* allele was PCR amplified with primers 311 and 312 using pKD4 as a template. Wild-type *fliC* of DY378 was disrupted by λ-red recombination of Δ*fliC*::*kan* allele and SK2462 strain was constructed (Datsenko and Wanner, 2000). Then Δ*fliC*::*kan* allele was transferred to wild-type MG1655 by P1 transduction with SK2462 lysate to construct SK2468 (Thomason et al., 2007).

Deletion mutant in *Lm* was constructed using pLR16-Phes as previously described (Argov et al., 2017). In brief, pLR16-AB1 was transformed into *E. coli* SM-10 strain and subsequently transferred to *Lm* 10403S by conjugation. *Lm* transconjugants were selected by plating on LB agar plates supplemented with 2% glucose and containing 7.5 μg/ml chloramphenicol and 100 μg/ml Streptomycin. Transconjugants were then passaged in LB supplemented with 2% glucose and plated to obtain single colonies. Colonies were tested for sensitivity to chloramphenicol. Chloramphenicol sensitive colonies were further verified to contain the desired mutation by PCR. For disruption of the *flaA* gene, pSH22 was transformed into *E. coli* SM-10 strain and transferred to *Lm* 10403S by conjugation. *Lm* transconjugants were selected by plating on LB agar plates supplemented with 2% glucose and containing 7.5 μg/ml chloramphenicol and 100 μg/ml Streptomycin. Transconjugants were then passaged in LB supplemented with 2% glucose and 10 μg/ml chloramphenicol at 41°C and plated to obtain *flaA* disruption mutants.

Details on plasmid construction

Plasmid constructions were performed in *E. coli* DH5α using standard methods.

pSH13 (*flhA-GFP-kan*) was constructed by amplifying the 3′ region of *flhA* using the gDNA of wild-type *Bs* strain PY79, using primers *flhA* CT-F-EcoRI and *flhA* CT-R-*Xho*I. The PCR-amplified DNA was digested with EcoRI and *Xho*I and was cloned into pKL168 digested with the same enzymes.

pSH17 (*amyE*::$P_{hyper\text{-}spank}$-$fliP_{2xHA}$-*spec*) was constructed by amplifying *fliP* using the gDNA of wild-type *Bs* strain PY79, using primers *fliP* ORF F (*Hind*III) and *fliP* ORF R (2xHA), followed by a second round of PCR using primers *fliP* ORF F (*Hind*III) and 2xHA R (*Sph*I). The PCR-amplified DNA was digested with *Hind*III and *Sph*I and was cloned into pDR111 digested with the same enzymes.

pSH19 (*amyE*::$P_{hyper\text{-}spank}$-$fliP_{2xHA\text{-}LOOP}$-*spec*) was constructed by amplifying the 5′ and 3′ regions of *fliP* using the gDNA of wild-type *Bs* strain PY79. 5′ region of *fliP* was amplified using primers *fliP* ORF F (pDR111) and *fliP* NT R (GSS/2xHA), and the 3′ region of *fliP* was amplified using primers *fliP* CT F (GSS/2xHA) and *fliP* CT R (pDR111). The PCR-amplified DNA was cloned into pDR111 digested with *Hind*III and *Sph*I using Gibson assembly kit (NEB, USA).

pSH21 [*amyE*::$P_{hyper\text{-}spank}$-*CORE*-F_{Ec} (*fliOPQR flhBA*)-*spec*] was constructed by amplifying the *Ec CORE* using the plasmid pRP7358, using primers *Ec fliO-flhA* F (pDR111) and *Ec fliO-flhA* R (pDR111). The PCR-amplified DNA was cloned into pDR111 digested with *Hind*III and *Sph*I using Gibson assembly kit (NEB, USA).

pLR16-AB1 was constructed by amplifying approximately 1000bp fragments upstream of *fliP* and downstream of *flhA* using primers *Lm CORE* P1-P2 and *Lm CORE* P3-P4 respectively. The fragments were joined using Gibson assembly kit (NEB, USA) and further amplified by PCR using primers *Lm CORE* P1 and P4. The resultant PCR product was digested with *Xho*I and SalI and cloned into pLR16-Phes digested with the same enzymes.

pSH22 (pLR16-*Lm flaA* int) was constructed by amplifying approximately 450bp fragment of the *Lm flaA* gene, using primers *Lm flaA* int F and *Lm flaA* int R. The PCR-amplified DNA was cloned into pLR16-Phes digested with SalI using Gibson assembly kit (NEB, USA).

pSH23 (pDG1514-*Bm hag* int) was constructed by amplifying approximately 450bp fragment of the *Bm hag* gene, using primers *Bm hag* int F (SalI) and *Bm hag* int R (BamHI). The PCR-amplified DNA was digested with SalI and BamHI and was cloned into pDG1514 digested with the same enzymes.

Nanotube visualization by XHR-SEM

Nanotube visualization was carried out as previously described (Dubey et al., 2016). Accordingly, *Bs*, *Bm*, *Ec* and *Lm* cells grown to mid logarithmic phase were spotted onto EM grids (mesh copper grids, EMS) placed over LB agar plates and incubated for 4 hr at 37°C. Cells were then washed 3 times with PBS × 1, fixed with 2% paraformaldehyde (Electron Microscopy Sciences) and 0.01% glutaraldehyde (Electron Microscopy Sciences) in sodium cacodylate buffer (0.1 M, pH 7.2, Electron Microscopy Sciences) for 10 min at 25°C. Cells were left overnight for fixation in 2% glutaraldehyde in sodium cacodylate buffer (0.1 M, pH 7.2) at 4°C. For cell dehydration, EM grids underwent a series of washes in increasing concentrations of ethanol (25, 50, 75, and 96%) (J.T.Baker) and kept in vacuum till visualization. Samples were coated and observed using Through-Lens Detector operated at Secondary Electron (TLD-SE) mode by Magellan XHR SEM (FEI).

Immuno-XHR-SEM analysis

Immuno-XHR-SEM analysis was carried out as previously described (Dubey et al., 2016; Stempler et al., 2017). *Bs* cells were grown on EM grids (mesh copper grids, EMS), and grid-attached cells were washed three times with PBS × 1, fixed with 2% paraformaldehyde and 0.01% glutaraldehyde in sodium cacodylate buffer (0.1 M, pH 7.2) for 10 min at 25°C. Subsequently, grids were washed 3 times in PBS × 1, incubated in PBS × 1 containing 2% BSA (Amresco) and 0.1% Tween 20 (J.T.Baker) for 30 min at 25°C, and washed twice with PBS × 1. Next, grids were incubated for 2 hr at 25°C with rabbit anti-HA antibodies (Thermo Fisher Scientific, USA) or rabbit anti-GFP, diluted 1:1000 in PBS × 1 containing 1% BSA. Grids were then washed 3 times with PBS × 1 and incubated for 1 hr at 25°C with 18nm gold-conjugated goat anti-rabbit antibodies (Jackson ImmunoResearch Laboratories, USA), diluted 1:500 in PBS × 1. Grids were washed 3 times with PBS × 1 and fixed with 2.5% glutaraldehyde in sodium cacodylate buffer (0.1 M, pH 7.2) for 1 hr at 25°C. Grids were then washed gently with water, and cells were dehydrated by exposure to a graded series of ethanol washes (25, 50, 75, 95, and 100% (× 2); 10 min each), samples were kept in vacuum till visualization. Specimens were imaged without coating by Magellan XHR SEM (FEI) using Through-Lens Detector operated at Secondary Electron (TLD-SE) and Low-voltage high-Contrast backscatter electron Detector (vCD).

Molecular exchange assay

For detecting molecular exchange, antibiotic transfer assay was carried out as described previously (Dubey and Ben-Yehuda, 2011) with some modifications. Donor and recipient strains used for the molecular exchange assays are listed in the Key resources table. Respective donor and recipient strains were grown to mid logarithmic phase, after which cells were mixed in 1:1 ratio (OD_{600} = 0.8 or 0.08) and incubated in LB supplemented with 1 mM IPTG for 4 hr at 37°C with gentle shaking. Equal numbers of cells were spotted onto either double selective LB plates containing chloramphenicol (6 μg/ml) and kanamycin (5 μg/ml) for detection of protein exchange, or triple selective LB plates containing chloramphenicol, kanamycin and lincomycin (25 μg/ml) for detection of plasmid exchange. As a control, cells were spotted onto LB plates lacking antibiotics. Plates were incubated at 37°C.

Motility assay

Motility assay was carried out as previously described (Kearns and Losick, 2003) with some modifications. Cells were grown to mid logarithmic phase in LB and concentrated 10 times to OD_{600} 5.0. 5 μL of the cell suspension was spotted on freshly prepared LB plates containing 0.3% agar, incubated at 37°C for 7-9 hr, and imaged over time.

Fluorescence microscopy

For visualization of FlhA-GFP, SpoIVFB-GFP and YueB-YFP, exponentially growing cells were harvested at an OD_{600} 0.5, washed with PBS × 1 and observed by fluorescence microscopy. For staining bacterial membrane and nanotubes, exponentially growing cells were harvested and resuspended in PBS × 1 containing 1 μg/ml FM4-64 (Molecular Probes, Thermo Fisher Scientific) and visualized by fluorescence microscopy. *Bs-Bm* competition assays were carried out as described previously (Stempler et al., 2017). Overnight cultures of *Bs* and *Bm* were diluted to OD_{600} 0.1, mixed, and mounted onto a metal ring (A-7816, Invitrogen) filled with

LB agarose (1.5%). Cells were incubated in a temperature-controlled chamber at 37°C, and followed by fluorescence microscopy. Cells were visualized by Eclipse Ti microscope (Nikon, Japan), equipped with CoolSnap HQII camera (Photometrics, Roper Scientific, USA). System control and image processing were performed with NIS Elements AR 4.3 (Nikon, Japan).

RNA isolation and qRT-PCR

RNA was extracted from *Bs* cells grown to the mid logarithmic phase by FastRNA Pro Blue kit (MP Biomedicals) according to the manufacturer protocol. RNA concentration was determined using NanoDrop 2000C (Thermo Scientific). 2 μg RNA from each sample was treated with RQ1 DNase (2 Units, Promega), and subjected to cDNA synthesis using qScript cDNA synthesis kit (Quanta Biosciences), according to the manufacturer protocol. qRT-PCR reactions were conducted using PerfeCTa SYBR Green FastMix (Quanta Biosciences), and fluorescence detection was performed using Applied Biosystems StepOnePlus system according to manufacturer instructions. RNA from 16S rRNA was used to normalize expression. Relative gene expression and melt curve analysis was done using the Applied Biosystems StepOnePlus software (v. 2.3). Each assay was performed in duplicates with at least two RNA templates prepared from independent biological repeats. qRT-PCR primers were designed using Primer3 software (v. 0.4.0, available online).

Phylogenetic analysis

In order to study the evolutionary conservation of the CORE complex we focused on seven proteins of *Bs* 168: the five CORE complex proteins and two exclusive proteins of the flagellar apparatus. In addition, we analyzed three proteins from *E. coli* O157:H7 *str.* EDL933 and one protein from *C. trachomatis* D/UW-3/CX, which are unique to the T3SS. These were searched in each of the core genomes in the STRING database, using STRING's protein homology data (Szklarczyk et al., 2017) and analyzed by custom python scripts to determine the conservation of the query proteins (Table S2). Sequence similarity scores < 0.1 were discarded. The conservation vectors of the species in each phylum were clustered using hierarchical clustering (Figure S5). Additionally, all species from all phyla were clustered together, and species clustering along with *M. fulvus* were inspected further to assess whether they include only the CORE proteins without other T3SS or flagella proteins, in a similar manner to *M. fulvus*.

PSI-BLAST was used to search several flagella unique proteins from *Bs*, along with several T3SS unique proteins from both Enterohemorrhagic *E. coli* and *C. trachomatis*, against the proteomes of the suspected species from the NCBI Assembly database. Hits adhering to stringent threshold of E-value < 0.01, spanning longer than half the length of the query with identity > 0.2, were considered putative homologs. Furthermore, a literature search was carried out by searching PubMed for the relevant species names alongside "Type III secretion system" and "flagella." Species that had putative hits for < 20% of the proteins in all categories and had no relevant results in the literature search were considered to harbor only the CORE proteins.

QUANTIFICATION AND STATISTICAL ANALYSIS

Unless stated otherwise, bar charts display a mean ± SD from at least 3 independent biological experiments. Quantification of nanotubes were done manually. MS Excel was used for all statistical analysis, data processing and presentation.

Cell Reports, Volume *27*

Supplemental Information

A Ubiquitous Platform

for Bacterial Nanotube Biogenesis

Saurabh Bhattacharya, Amit K. Baidya, Ritesh Ranjan Pal, Gideon Mamou, Yair E. Gatt, Hanah Margalit, Ilan Rosenshine, and Sigal Ben-Yehuda

Supplemental information

Supplementary Figures

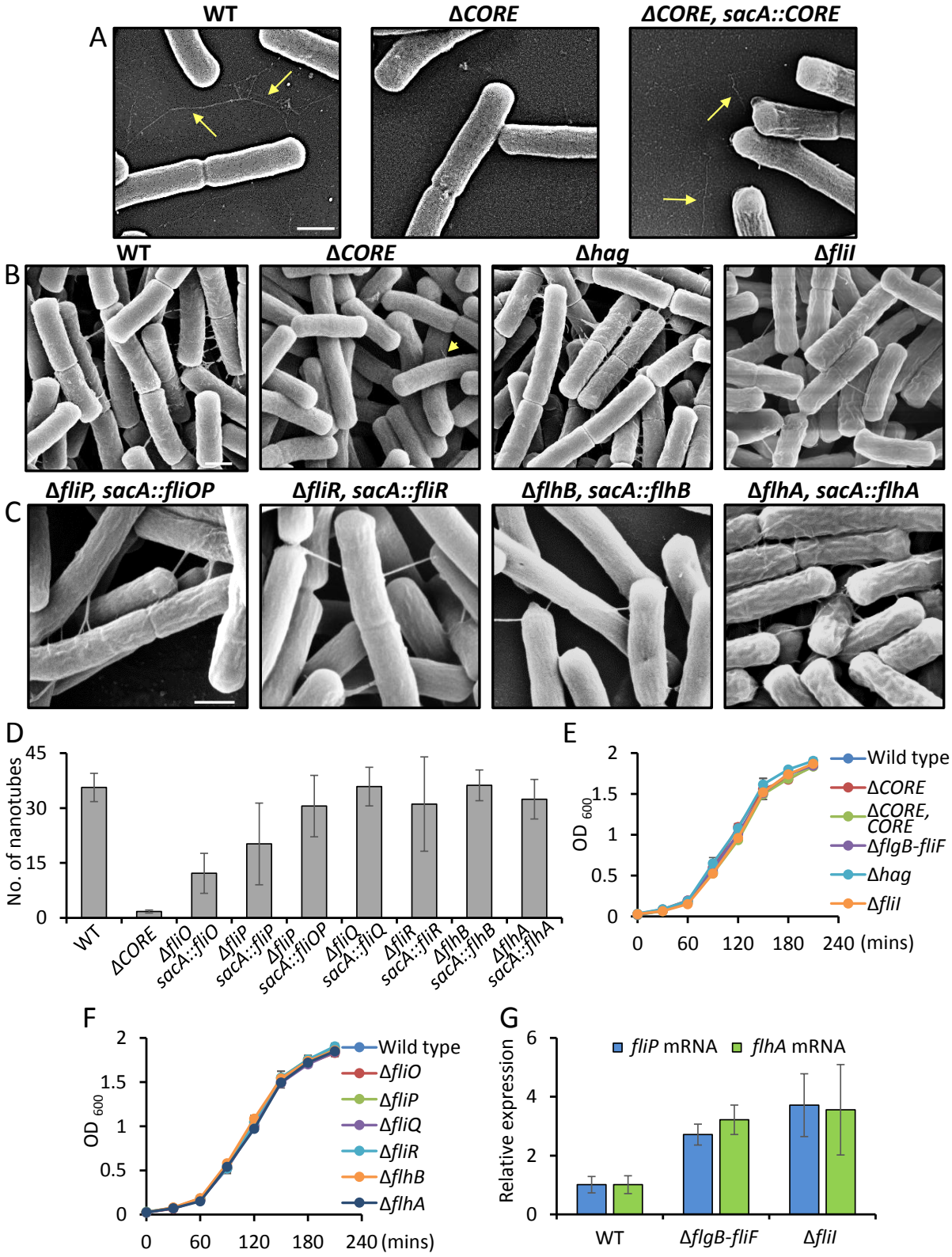

Figure S1: *Bs CORE* mutants are impaired in nanotube formation. Related to Figures 1 and 2
(**A**) PY79 (wild type), SH9 (Δ*CORE*) and SH33 (Δ*CORE*, *sacA::CORE*) strains were visualized by XHR-SEM to monitor the formation of extending nanotubes at low cell density. Strains were grown to mid logarithmic

phase, spotted onto EM grids at low cell density (x0.1 dilution), incubated on LB agar plates for 2 hrs at 37°C, and visualized by XHR-SEM. Arrows indicate extending nanotubes. Scale bar represents 500 nm.
(**B**) The indicated *Bs* mutant strains were visualized by XHR-SEM to monitor the formation of intercellular nanotubes. Strains were grown to mid logarithmic phase, spotted onto EM grids, incubated on LB agar plates for 4 hrs at 37°C, and visualized by XHR-SEM. PY79 (wild type) and SH9 (Δ*CORE*) are larger fields of the images displayed in Figure 1C. Scale bar represents 500 nm.
(**C**) *Bs CORE* mutants were complemented with the corresponding *CORE* genes, as indicated, and were visualized by XHR-SEM to monitor the formation of intercellular nanotubes. Cells were processed for XHR-SEM as in (B). Shown are representative examples of the indicated complemented strains. Scale bar represents 500 nm.
(**D**) Quantification of the average number of nanotubes displayed per 50 cells by the indicated strains following XHR-SEM analysis described in (C). Shown are average values and SD of at least 3 independent experiments ($n \geq 200$ for each strain).
(**E-F**) Growth kinetics of *Bs CORE* mutants. The indicated mutant strains were incubated in LB medium at 37°C and cell growth was followed by measuring OD_{600} at the indicated time points.
(**G**) Expression of *CORE* genes in *Bs* non-*CORE* flagellar basal body mutants. RNA was isolated from *Bs* wild type (PY79), Δ*flgB-fliF* (SH8) and Δ*fliI* (SH177) cells grown to the mid logarithmic phase and the expression of *fliP and flhA* was determined by qRT-PCR. Transcript levels are relative to wild type (PY79). Each bar represents an average value and SD of three independent experiments.

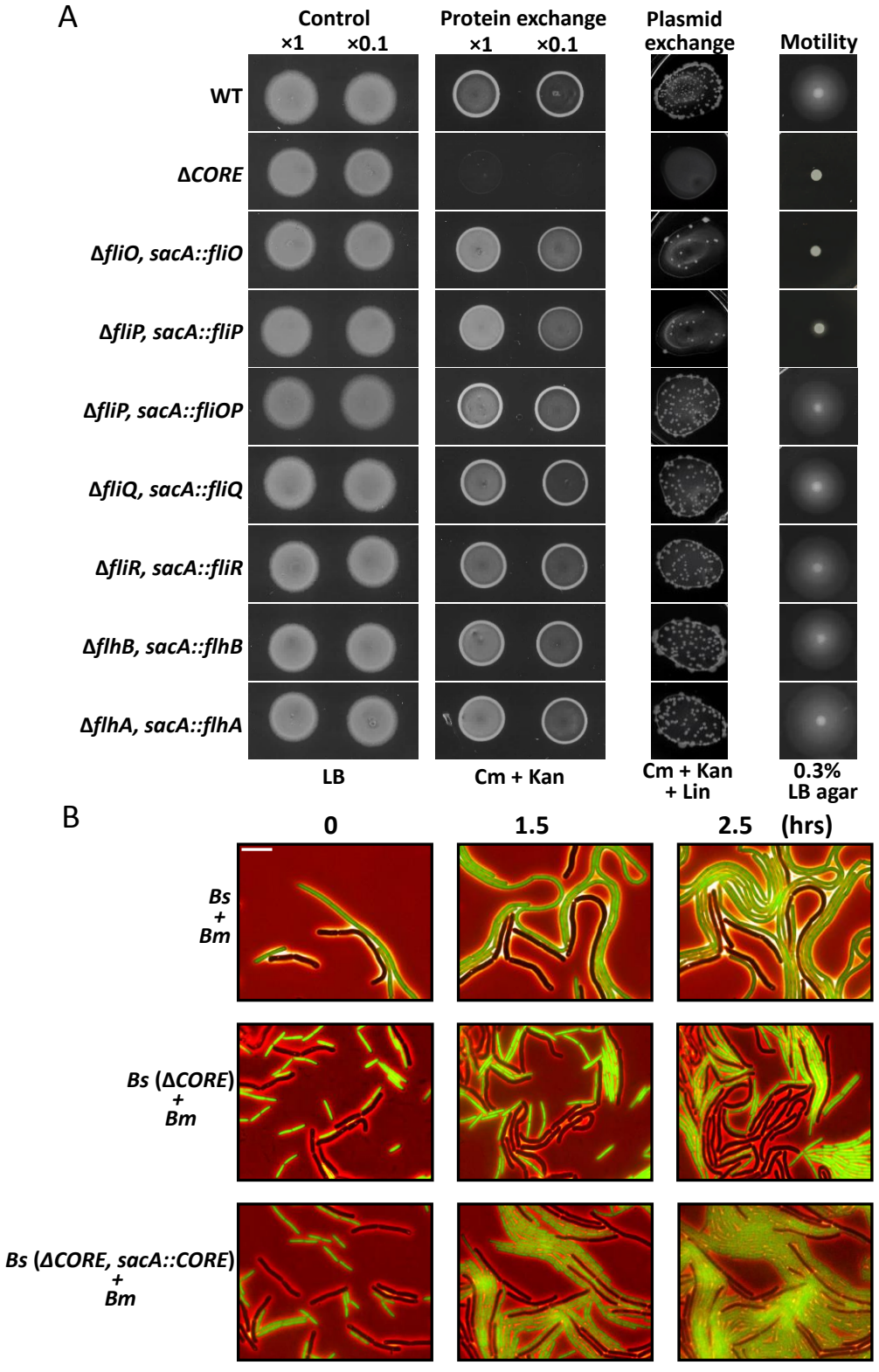

Figure S2: *Bs CORE* mutants are impaired in nanotube mediated molecular exchange. Related to Figure 2

(**A**) Assessing molecular exchange in *Bs CORE* complemented strains. For protein exchange assay, pairs of a donor (SB463: *amyE*::$P_{hyper\text{-}spank}$-*cat-spec*) (Cm^R, $Spec^R$) and a recipient (SB513: *amyE*::$P_{hyper\text{-}spank}$-*gfp-kan*) (Kan^R) parental strains (wild type) were used. The investigated complemented strains harbor the corresponding genotypes of both donor and recipient strains. Donor and recipient strains were mixed in 1:1 ratio (at two concentrations x1, x0.1) and incubated in LB supplemented with 1 mM IPTG for 4 hrs at 37°C with gentle

shaking. Equal numbers of cells were then spotted onto LB agar (Control) and LB agar containing chloramphenicol (Cm) and kanamycin (Kan) (Protein exchange), and photographed after 18 hrs. For plasmid exchange assay, pairs of a donor (GD110: *amyE*::$P_{hyper\text{-}spank}$-*cat-spec*, pHB201/*cat, erm*) (Cm^R, $Spec^R$, Mls^R) and a recipient (SB513: *amyE*::$P_{hyper\text{-}spank}$-*gfp-kan*) (Kan^R) parental strains (wild type) were used. The investigated complemented strains harbor the corresponding genotypes of both donor and recipient strains. Cells were mixed in 1:1 ratio (concentration x1), processed as described for protein exchange, and spotted onto LB agar containing Cm, Kan and lincomycin (Lin) (Plasmid exchange). Cells were incubated at 37ºC and colonies were photographed after 36 hrs of incubation. For motility assay, wild type (PY79) and the indicated strains were grown to the mid logarithmic phase and spotted onto LB plates containing 0.3% agar and photographed after 7 hrs of incubation at 37ºC (Motility).

(**B**) *Bm* inhibition by *Bs* is CORE dependent. Representative time lapse microscopy images displaying mixtures of *Bs* (AR16: *amyE*::P_{rrnE}-*gfp*) and *Bm* (OS2) (upper panels), *Bs* (SH30: Δ*CORE*, *amyE*::P_{rrnE}-*gfp*) and *Bm* (OS2) (middle panels), and *Bs* (SH41: Δ*CORE, sacA::CORE, amyE*::$P_{hyper\text{-}spank}$-*gfp*) and *Bm* (OS2) (lower panels). Shown are overlay of fluorescence from GFP (green) and phase contrast (red) images, captured at the indicated time points. *Bs* cells are shown in green while *Bm* cells are shown in black. Scale bar represents 5 μm.

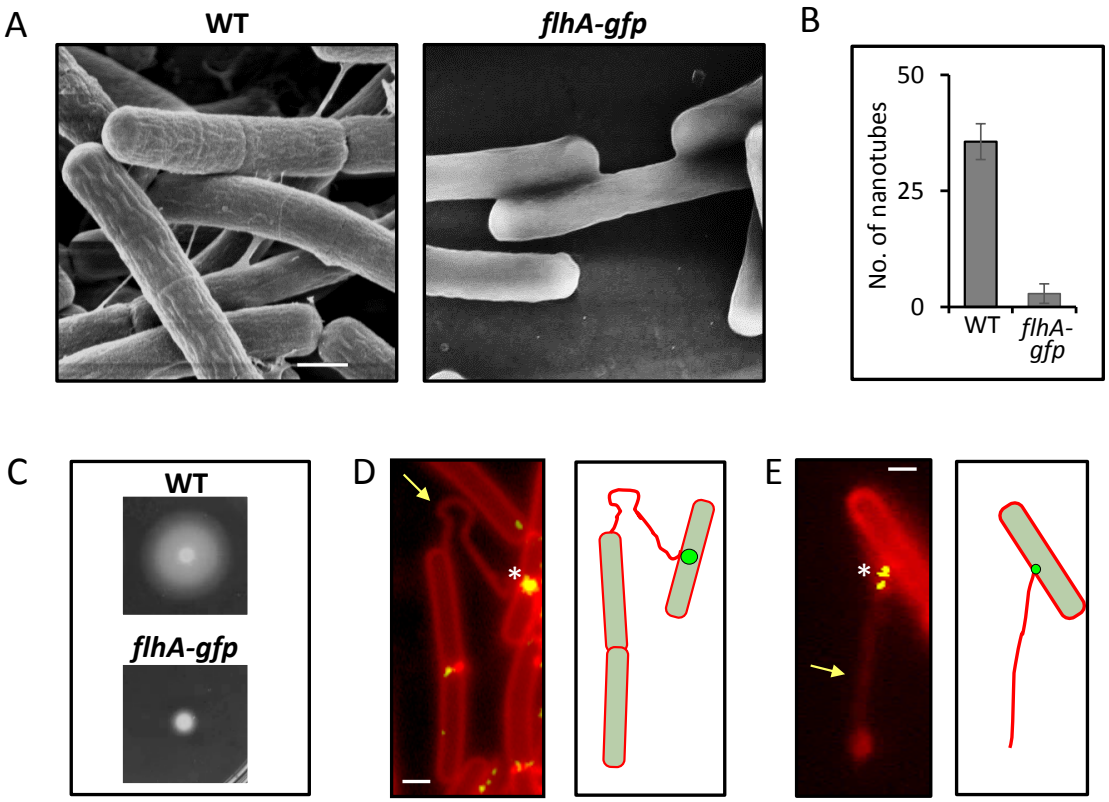

Figure S3: FlhA localizes to the base of nanotubes. Related to Figure 3
(**A**) WT (PY79) and SH47 (*flhA-gfp*) strains were visualized by XHR-SEM to monitor the formation of intercellular nanotubes. Strains were grown to mid logarithmic phase, spotted onto EM grids, incubated on LB agar plates for 4 hrs at 37°C, and visualized by XHR-SEM. Scale bar represents 0.5 µm.
(**B**) Quantification of the average number of nanotubes displayed per 50 cells by the indicated strains following XHR-SEM analysis described in (A). Shown are average values and SD of at least 3 independent experiments (n≥70 for each strain).
(**C**) Motility assay for PY79 (wild type) and SH47 (*flhA-gfp*) strains. Cells were grown to mid logarithmic phase, spotted onto LB plates containing 0.3% agar, and photographed after 7 hrs of incubation at 37ºC.
(**D-E**) SH55 (*flhA-gfp*, *amyE*::$P_{hyper\text{-}spank}$-*ymdB*, Δ*ymdB*, Δ*hag*) cells were grown in liquid LB to mid logarithmic phase, stained with a membrane dye (FM 4-64) and visualized by fluorescence microscopy. Shown are overlays of signals from FlhA-GFP (green) and FM 4-64 (red). Arrows denote nanotubes, and asterisks highlight FlhA foci at sites proximal to nanotube emanation. Schematics depict cells and nanotubes layouts (red), as well as FlhA-GFP signal (green) at sites of nanotube origin. Scale bars represent 0.5 µm.

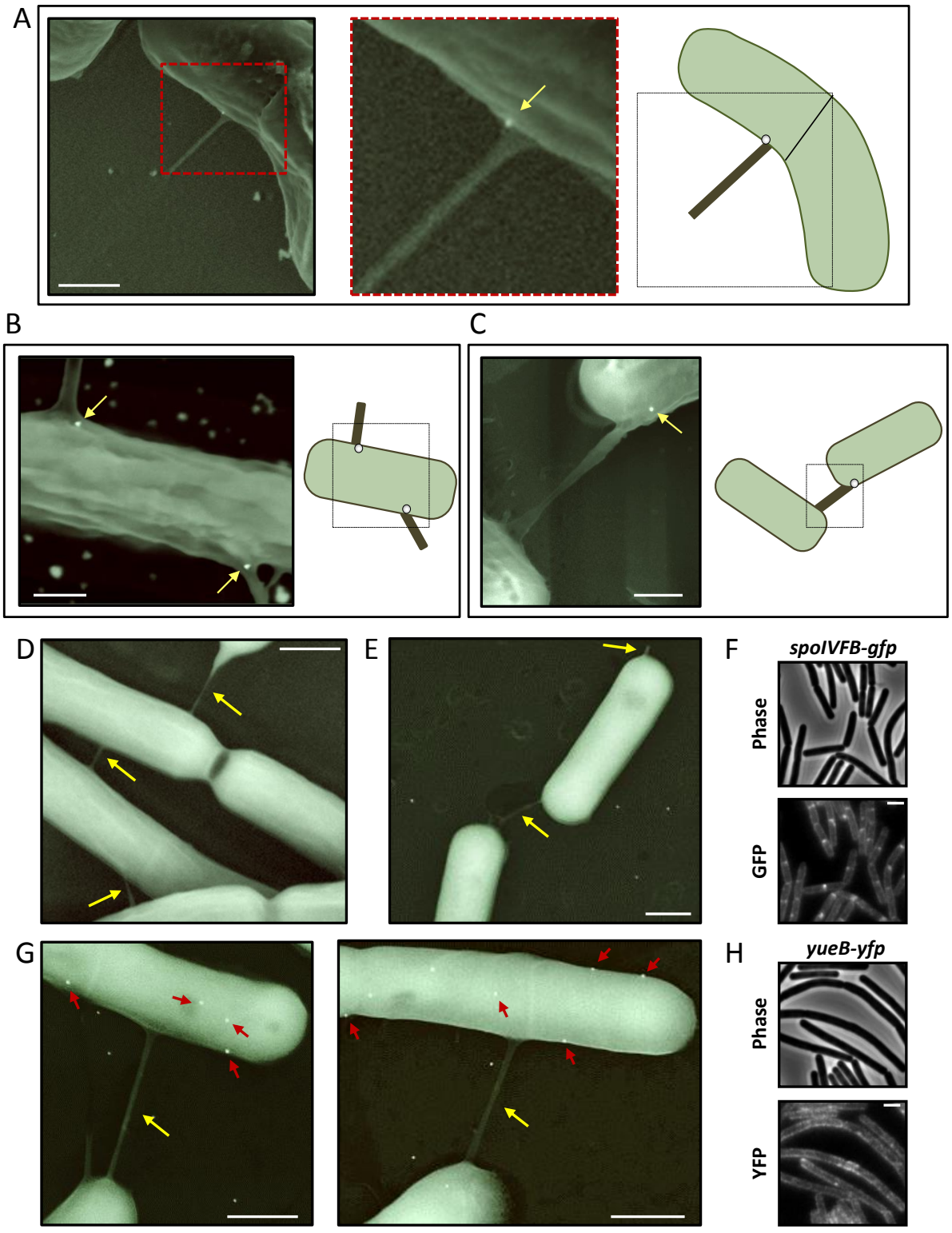

Figure S4: FliP localizes to sites of nanotube emanation. Related to Figure 3
(**A**) Cells expressing HA tagged FliP (SH110: *amyE*::P$_{hyper\text{-}spank}$-*fliP*$_{2xHA}$, *sacA*::P$_{hyper\text{-}spank}$-*ymdB, Δmbl*) were spotted onto EM grids and subjected to immuno-gold XHR-SEM using primary antibodies against HA and secondary gold-conjugated antibodies. Samples were not coated before observation. Shown are overlays of XHR-SEM images that were acquired using TLD-SE (Through lens detector- secondary electron) for nanotube visualization and vCD (low-kV high-contrast detector) for gold particle detection. An example of FliP$_{2xHA}$

localization (white dot), at the site of emergence of an extending nanotube is displayed. Right panel is a magnification of the red inset in the left panel. Scale bar represents 250 nm.
(**B**) An example of $FliP_{2xHA\text{-}LOOP}$ localization (white dots), at the sites of nanotube emergence. SH161 (*amyE*::$P_{hyper\text{-}spank}$-*fliP*$_{2xHA\text{-}LOOP}$-*spec*, *sacA*::$P_{hyper\text{-}spank}$-*ymdB-kan*, *Δmbl::erm*) cells were processed for immuno XHR-SEM as in (A). Shown is an overlay image of TLD-SE and vCD modes. Scale bar represents 250 nm.
(**C**) An example of localization of $FliP_{2xHA}$ (white dot) expressed as a sole copy, at the site of nanotube emergence. SH247 (Δ*fliP::tet*, $P_{fla/che}$-*fliQ-cheD*, *sacA::*$P_{fla/che}$-*fliO-fliP*$_{2xHA}$-*spec, Δmbl::erm*) cells were processed for immuno XHR-SEM as in (A). Shown is an overlay image of TLD-SE and vCD modes. Scale bar represents 250 nm.
Schematics in (A-C) depict the interpretive cell layout and highlights the nanotube region with gold signal (black dashed box) captured by XHR-SEM. Arrows indicate gold signal from HA-tagged FliP.
(**D**) GB168 (*ΔymdB, Δhag, amyE*::$P_{hyper\text{-}spank}$-*ymdB*) cells, lacking HA tag, were processed for immuno XHR-SEM as in (A). Shown is an example of an overlay of XHR-SEM images that were acquired using TLD-SE and vCD modes. No gold signal was obtained from cell surface and/or nanotubes. Arrows indicate nanotubes. Scale bar represents 500 nm.
(**E**) SH258 (*amyE*::P_{xylA}-*spoIVFB-gfp-cat*, *sacA*::$P_{hyper\text{-}spank}$-*ymdB-kan, Δmbl::erm*) cells, were spotted onto EM grids and subjected to immuno-gold XHR-SEM using primary antibodies against GFP and secondary gold-conjugated antibodies. Samples were not coated before observation. Shown is an example of an overlay of XHR-SEM images that were acquired using TLD-SE and vCD modes. No gold signal was obtained from cell surface and/or nanotubes. Arrows indicate nanotubes. Scale bar represents 500 nm.
(**F**) BDR524 (*amyE*::P_{xylA}-*spoIVFB-gfp-cat*) cells were grown in liquid LB to mid logarithmic phase and visualized by fluorescence microscopy. Shown are images from phase contrast and GFP fluorescence. SpoIVFB-GFP protein localizes to the cell membrane facing the cytoplasm. Scale bar represents 1 μm.
(**G**) SH257 (*amyE*::$P_{hyper\text{-}spank}$-*yueB-yfp-spec*, *sacA*::$P_{hyper\text{-}spank}$-*ymdB-kan, Δmbl::erm*) cells, were processed for immuno XHR-SEM as in (E). Shown are examples of overlays of XHR-SEM images that were acquired using TLD-SE and vCD. Yellow arrows indicate nanotubes. Red arrows indicate signal from YueB-YFP. Scale bar represents 500 nm.
(**H**) ET13 (*amyE*::$P_{hyper\text{-}spank}$-*yueB-yfp-spec*) cells were grown in liquid LB to mid logarithmic phase and visualized by fluorescence microscopy. Shown are images from phase contrast and YFP fluorescence. YueB-YFP receptor protein localizes to the cell circumference. Scale bar represents 1 μm.

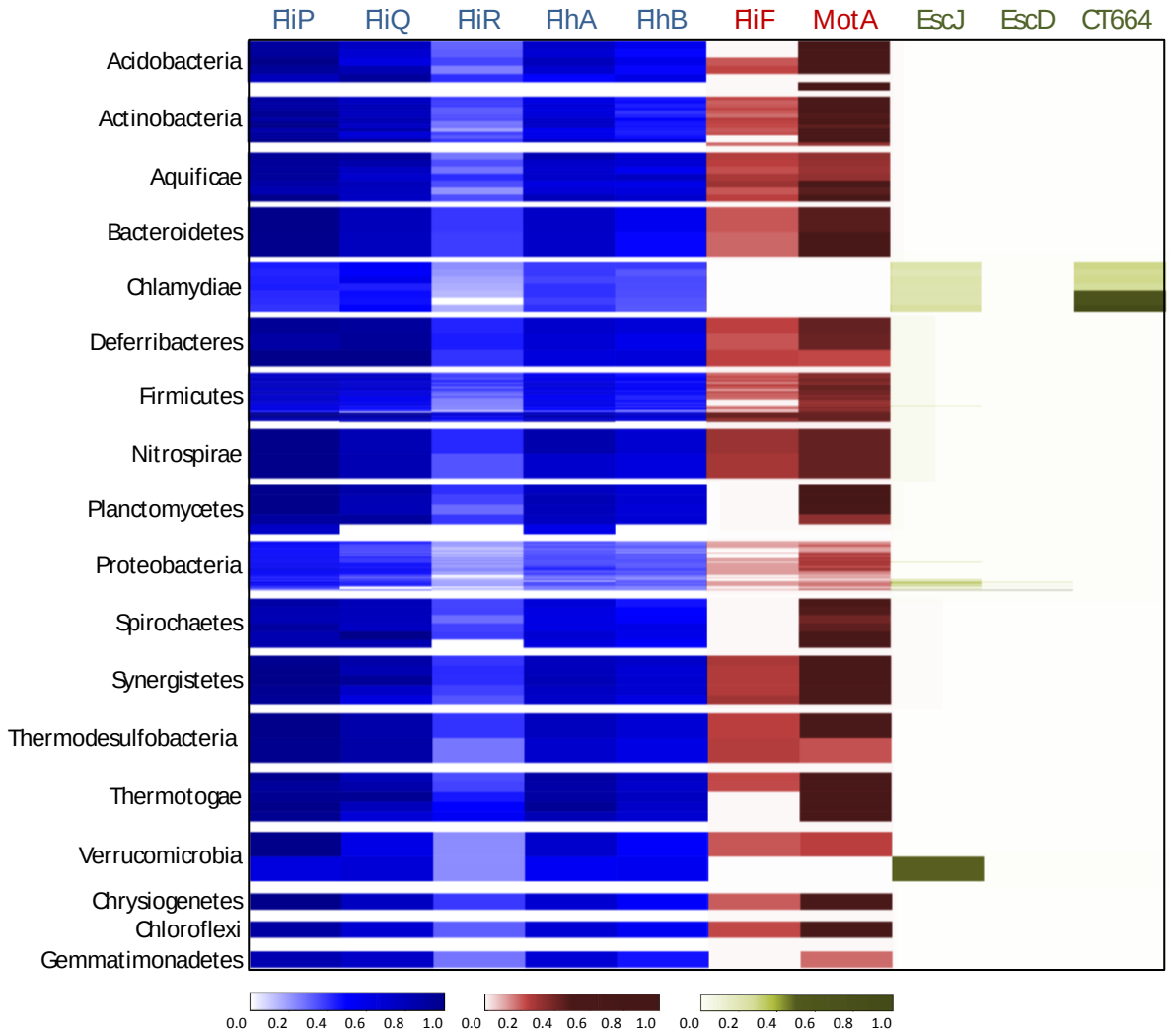

Figure S5: The spread of CORE complex in diverse bacterial phyla. Related to Figure 4
Heatmap showing the conservation of proteins comprising flagella or injectisome in different bacterial phyla. Each row depicts a single species from the STRING database representative genomes, which is included in the respective phylum listed on the left. Each column represents a single protein (blue: CORE proteins; red: exclusive proteins of the flagella apparatus; green: proteins that are unique to the injectisome apparatus). The proteins used as a reference derived from *Bs* flagella (blue and red proteins), from Enterohemorrhagic *E. coli* injectisome (EscJ,D) and from *C. trachomatis* injectisome (CT664). The sequence similarity scores are based on homology data extracted from the STRING database. Color ranges at the bottom represent the STRING sequence similarity scores. See also Table S2 for detailed analysis.

Table S1: Conservation of CORE proteins in distinct bacterial species. Related to Figure 4
Conservation analysis of CORE proteins in *Bm* (DSM319), *Lm* (10403S) and *Ec* (K12 MG1655) by NCBI Protein BLAST, using the corresponding *Bs* PY79 CORE protein sequences as query.

		Bm	***Lm***	***Ec***
FliO	Query Coverage (%)	82	-	10
	Identities (%)	36	-	36
	Positives (%)	62	-	48
	E- value	$7e^{-32}$	-	1.2
FliP	Query Coverage (%)	100	95	95
	Identities (%)	79	34	54
	Positives (%)	92	62	72
	E- value	$2e^{-130}$	$3e^{-45}$	$2e^{-76}$
FliQ	Query Coverage (%)	100	50	100
	Identities (%)	72	44	51
	Positives (%)	88	62	69
	E- value	$1e^{-38}$	$5e^{-08}$	$4e^{-14}$
FliR	Query Coverage (%)	99	91	88
	Identities (%)	55	24	28
	Positives (%)	75	49	50
	E- value	$5e^{-86}$	$1e^{-16}$	$1e^{-16}$
FlhB	Query Coverage (%)	99	93	95
	Identities (%)	59	34	39
	Positives (%)	76	59	62
	E- value	$7e^{-149}$	$3e^{-62}$	$3e^{-73}$
FlhA	Query Coverage (%)	100	99	97
	Identities (%)	97	36	45
	Positives (%)	86	59	64
	E- value	0	$3e^{-128}$	$3e^{-175}$

Table S2: Table showing the conservation of proteins comprising different flagella or type III secretion system (T3SS) subunits in different bacterial species. Related to Figure 4

(Provided as a separate Excel file)

Each row represents a single species from the STRING core genomes and each column represents one protein. The protein names are followed by the species of origin (Bacillus: *B. subtilis* proteins; EHEC: Enterohemorrhagic *E. coli* proteins; Chlamydia: *C. trachomatis* protein). The sequence similarity scores are based on the STRING database homology data. Species lacking any homolog were excluded from the analysis.

Table S3. List of primers used in this study. Related to STAR Methods

Primer name	**Primer sequence (5'-3')**
P_{flgB}1	GTTGACCAGTGCTCCCTGCAATAAGCTTTATTTCCTGGGTTG
P_{flgB}2	GCTCAAATCCACTTACCTCCA
flgB-fliF KO P1	CCAGCAAATTGAAAATGATCG
flgB-fliF KO P2	CTGAGCGAGGGAGCAGAACAAATCCACTTACCTCCATTTCA
flgB-fliF KO P3	TGGAGGTAAGTGGATTTGAGCATGGCGAGACGTGATCAAGATA
flgB-fliF KO P4	ATATCATCCCCTCCGCCTCT
CORE KO P1	TGATGATGAAATGCTGGTGAA
CORE KO P2	CTGAGCGAGGGAGCAGAATTTCAACAGTCGTACACCCTTT
CORE KO P3	TGGAGGTAAGTGGATTTGAGCATGAAAATAAAAAAATTTACTGCTGCT
CORE KO P4	CACATTCTGGCCGTTAGTCA
sacA P1	CAGCATTTTCCGCTTTTCTC
sacA P2	AGCCTGCCCTTTCAAATTCT
sacA P3	GTTGACCAGTGCTCCCTGTGTTTTCCCTTCAAGGATCG
sacA P4	TTTTCCAAACATTCCGGTGT
Comp P_{flgB}1	AGAATTTGAAAGGGCAGGCTCAATAAGCTTTATTTCCTGGGTTG
Comp P_{flgB}2	CAATAAAATATTGACTCTTTTTCATGCTCAAATCCACTTACCTCCA
Comp P_{flgB}2a	GCACAGTAGCATGGTTATTCATGCTCAAATCCACTTACCTCCA
Comp P_{flgB}R	GCTCAAATCCACTTACCTCCA
Bs CORE comp1	ATGAAAAAGAGTCAATATTTTATTG
Bs CORE comp2	CTGAGCGAGGGAGCAGAATTAAATATCCACCACTCCAATG
Comp P_{HS}1	AGAATTTGAAAGGGCAGGCTCTCGAGGGTAAATGTGAGCA
Comp P_{HS}2	CAATAAAATATTGACTCTTTTTCATCATAGTAGTTCACCACCTTTAAGC
ymdB R	CTGAGCGAGGGAGCAGAACTATTCAAAGAACATGTGATCATCG
fliO KO P1	TGATGATGAAATGCTGGTGAA
fliO KO P2	CTGAGCGAGGGAGCAGAATTTCAACAGTCGTACACCCTTT
fliO KO P3	TGGAGGTAAGTGGATTTGAGCATGAATGAGTTTATAAATATTTTCAGTTC
fliO KO P4	AAAAAGCAGGAAATAAGTCAATAA
fliP KO P1	GCAGCATTTATGCGAATGAT
fliP KO P2	CTGAGCGAGGGAGCAGAAGATGACGTGGGCCTTTCTT
fliP KO P3	TGGAGGTAAGTGGATTTGAGCGTGAGTTCAGAATTTGTAATTTCTATGG
fliP KO P4	AAAACATTCCGGACAACGAC
fliQ KO P1	AATATTGGCGGCACATCG
fliQ KO P2	CTGAGCGAGGGAGCAGAAAACTCACGTTTAGCACCTACCC
fliQ KO P3	TGGAGGTAAGTGGATTTGAGCATGAATTCAATTATTGACTTATTTCCTGC
fliQ KO P4	TCATTGTGAGCGATTCGGTA
fliR KO P1	AACAAAACCGTTCTGAAGGAAA
fliR KO P2	CTGAGCGAGGGAGCAGAATTCATCTCTACATTACCCTGCAAA
fliR KO P3	TGGAGGTAAGTGGATTTGAGCATGAAGCTTAGAGTTGACCTGCAG
fliR KO P4	GCCTGGTCAATTTCCACTTG
flhB KO P1	CGGGCCATTATTGGCTATT
flhB KO P2	CTGAGCGAGGGAGCAGAACTTCATTAAGAAACACCGACCA
flhB KO P3	TGGAGGTAAGTGGATTTGAGCATGTCAACAAGAGATTTATCCGTT
flhB KO P4	GAACAACACTTTCAGGGCTTTT
flhA KO P1	CCGCCGTTTCTTTACTGGT
flhA KO P2	CTGAGCGAGGGAGCAGAACTCTTGTTGACATGCTGTTTTT
flhA KO P3	TGGAGGTAAGTGGATTTGAGCATGAAAATAAAAAAATTTACTGCTGCT
flhA KO P4	CACATTCTGGCCGTTAGTCA
Ec CORE comp1	ATGAATAACCATGCTACTGTGC
Ec CORE comp2	CTGAGCGAGGGAGCAGAACTTGCACCAGCAGCGGAAAC
fliI KO P1	GAGAGTCATTCGCGATGTTG
fliI KO P2	CTGAGCGAGGGAGCAGAATCAGCTGCACCTGCTTCC
fliI KO P3	TGGAGGTAAGTGGATTTGAGCGTGGCTTATCAATTTAGATTCCAAAAG
fliI KO P4	ATAGGTTGCTGCTTGCTCAG
flhA CT-F-*Eco*RI	TAGTAGGAATTCCAGTAGTTGATCCTGCATCAGTC
flhA CT-R-*Xho*I	CTACTACTCGAGAATATCCACCACTCCAATGCTT

fliP ORF F (*Hind*III)	AAACCCAAGCTTAAAGGTGGTGAACTACTATGAATGAGTTTATAAATATTTTCAGTTC
fliP ORF R (2X HA)	CATAGGGATAGCCAGCGTAATCTGGAACATCATATGGGTAAAAGCTCTGAAGCAAAGATTTC
2X HA R (*Sph*I)	ACCTAGGCATGCTTATGCGTAGTCCGGGACGTCATAGGGATAGCCAGCGTAA
2X HA R	CTGAGCGAGGGAGCAGAATTATGCGTAGTCCGGGACGTCATAGGGATAGCCAGCGTAA
fliP ORF F (pDR111)	AATTGTGAGCGGATAACAATTAAGCTTAAAGGTGGTGAACTACTATGAATGAGTTTATAAATATTTTCAGTTC
fliP NT R (GSS/2X HA)	CATAGGGATAGCCAGCGTAATCTGGAACATCATATGGGTAGGAACTACCATCCATTTTCGCGTAATTCA
fliP CT F (GSS/2X HA)	TTACGCTGGCTATCCCTATGACGTCCCGGACTACGCAGGATCGAGTAAACCTGAATCATTAAAGGATATT
fliP CT R (pDR111)	CCACCGAATTAGCTTGCATGCCTAAAAGCTCTGAAGCAAAGA
Ec fliO-flhA F (pDR111)	AATTGTGAGCGGATAACAATTAAGCTTAAAGGTGGTGAACTACTATGAATAACCATGCTACTGTGC
Ec fliO-flhA R (pDR111)	CCACCGAATTAGCTTGCATGCCTTGCACCAGCAGCGGAAAC
Lm CORE P1	CCCAAACTCGAGTCAGAGATATCAAGGACTTTC
Lm CORE P2	ATCTTTTCTACTAAATGTTTTCCCATTGCCTTAGTCTCCTCTTTCAAAAG
Lm CORE P3	CTTTTGAAAGAGGAGACTAAGG CAATGGGAAAACATTTAGTAGAAAAGAT
Lm CORE P4	AAACCCGTCGACCCAGAAGAAAATGTAAAGCACGTTA
fliO comp1	TGGAGGTAAGTGGATTTGAGCATGAAAAAGAGTCAATATTTTATTG
fliO comp2	CTGAGCGAGGGAGCAGAATCATTCATGATGACGTGG
fliP comp1	TGGAGGTAAGTGGATTTGAGCATGAATGAGTTTATAAATATTTTCAGTTC
fliP comp2	CTGAGCGAGGGAGCAGAACTAAAAGCTCTGAAGCAAAGATTTC
fliQ comp1	TGGAGGTAAGTGGATTTGAGCATGAGTTCAGAATTTGTAATTTCT
fliQ comp2	CTGAGCGAGGGAGCAGAATTACCCTGCAAAACGATTTA
fliR comp1	TGGAGGTAAGTGGATTTGAGCATGAATTCAATTATTGACTTATTTCC
fliR comp2	CTGAGCGAGGGAGCAGAATTAAGAAACACCGACCAATG
flhB comp1	TGGAGGTAAGTGGATTTGAGCATGAAGCTTAGAGTTGACCT
flhB comp2	CTGAGCGAGGGAGCAGAATCAATATACTTTTTGTTTTGTTTTATATACG
flhA comp1	TGGAGGTAAGTGGATTTGAGCATGTCAACAAGAGATTTATCCGTT
flhA comp2	CTGAGCGAGGGAGCAGAATTAAATATCCACCACTCCAATGC
Lm CORE comp1	TGGAGGTAAGTGGATTTGAGCATGCGTAAAATAGCCTCTAGACGA
Lm CORE comp2	CTGAGCGAGGGAGCAGAATCAAGTTGGTTCAATCAGTGC
Bm CORE comp1	TGGAGGTAAGTGGATTTGAGCATGCTGCGAAAGTTCGTAATTG
Bm CORE comp2	CTGAGCGAGGGAGCAGAATCAGATATCCACCACTCCAACA
Lm flaA int F	TACCGGGCCCCCCCTCGAGGTCGACCTTGCAACGTATGCGTCAAT
Lm flaA int R	TATCAAGCTTATCGATACCGCGATGGATTGATTGTTCACG
Bm hag int F (*Sal*I)	AAACCCGTCGACTCAGGTCAGCGCATTAACAA
Bm hag int R (*Bam*HI)	AAACCCGGATCCTAGCGGCATCTGCACTTAAA
311	GGTGGAAACCCAATACGTAATCAACGACTTGCAATATAGGATAACGAATCGTGTAGGCTGGAGCTGCTTC
312	ATCAGGCAATTTGGCGTTGCCGTCAGTCTCAGTTAATCAGGTTACAACGACATATGAATATCCTCCTTA
3907	ACCGATATCATTACCCCGTCCGAGCGGATGCGCCGCCTGAGCCGTTAGTGTCCTAATTTTTGTTGACACTCTATC
3908	GATATTATTTTTCGGATAATCCTTAGGGTAGCATGATAAACGTTACGGAAATCAAAGGGAAAACTGTCCATA
3909	GAAAGCGATTAATCCGCTGG
3912	GTCACATTATCCGTCAGTCG
3950	CATGATAAACGTTACGGAACACTAACGGCTCAGGCGGCGCATTCG
3951	CGAATGCGCCGCCTGAGCCGTTAGTGTTCCGTAACGTTTATCATG
3914	TTTGCGCTCTGGCATCATTTACGCTCAATACTCTTTCCAGGATTGGCGACTCCTAATTTTTGTTGACACTCTATC
3915	GCGGCTTGCACCAGCAGCGGAAACAATAATATTGCTAATAAGGCTCTCATATCAAAGGGAAAACTGTCCATA

3952	GTGGCTATGTGGTGAAGCC
3953	GCTAATAAGGTTCTCATGTCGCCAATCCTGGAAAGAG
3954	CTCTTTCCAGGATTGGCGACATGAGAACCTTATTAGC
3955	CGTGATCAAATCATGCCTGC

All primers were designed during this study, and synthesized by Integrated DNA Technologies (IDT).